Temporal analysis of relative distances (TARDIS) is a robust, parameter-free alternative to single-particle tracking

Nature Methods

Martens, Koen J.A.; Turkowyd, Bartosz; Hohlbein, Johannes; Endesfelder, Ulrike

https://doi.org/10.1038/s41592-023-02149-7

nature methods

Article

https://doi.org/10.1038/s41592-023-02149-7

Temporal analysis of relative distances (TARDIS) is a robust, parameter-free alternative to single-particle tracking

Received: 3 May 2023

Accepted: 8 December 2023

Published online: 15 January 2024

Check for updates

Koen J. A. Martens[1,2,3] ✉, Bartosz Turkowyd[1,2], Johannes Hohlbein[3,4] & Ulrike Endesfelder[1,2]

In single-particle tracking, individual particles are localized and tracked over time to probe their diffusion and molecular interactions. Temporal crossing of trajectories, blinking particles, and false-positive localizations present computational challenges that have remained difficult to overcome. Here we introduce a robust, parameter-free alternative to single-particle tracking: temporal analysis of relative distances (TARDIS). In TARDIS, an all-to-all distance analysis between localizations is performed with increasing temporal shifts. These pairwise distances represent either intraparticle distances originating from the same particle, or interparticle distances originating from unrelated particles, and are fitted analytically to obtain quantitative measures on particle dynamics. We showcase that TARDIS outperforms tracking algorithms, benchmarked on simulated and experimental data of varying complexity. We further show that TARDIS performs accurately in complex conditions characterized by high particle density, strong emitter blinking or false-positive localizations, and is in fact limited by the capabilities of localization algorithms. TARDIS' robustness enables fivefold shorter measurements without loss of information.

Single-particle tracking (SPT) is a powerful technique in which individual particles are followed through time to infer information about a conjugated particle of interest, or about the environment in which the particles are embedded[1–5]. By attaching a contrast agent, such as a fluorescent, scattering or reflecting probe, to a particle of interest, SPT can be used to assess molecular dynamics in vitro or in vivo. Applications of SPT include, but are not limited to, photo-activatable localization microscopy[6] (sptPALM) via photo-activatable organic fluorophore or fluorescent protein conjugation, or interferometric scattering microscopy via for example gold nanoparticle conjugation[7,8]. These methods enable SPT with <40 nm spatial accuracy and >100 Hz temporal resolution. However, cellular SPT is limited to using sptPALM with fluorescent proteins, which limits the trajectory length to around three to ten time points[6,9]. Alternatively, proteins of interest can be tagged with, for example, HaloTag or SnapTag-moieties[10,11] and subsequently labeled with suitable organic fluorophores. This approach increases trajectory length compared to fluorescent proteins, but nonspecifically bound fluorophores can provide spurious localizations and thus wrong trajectory data.

Analysis of sptPALM is generally divided in two steps: (1) detection of individual particles and localization with subpixel accuracy, and (2) temporal linking of these localizations to trajectories. Detection and super-resolved localization (step 1) has seen big improvements in the recent decade following breakthroughs in computational image analysis[12–15], machine learning[16–18] and microscopy hardware design[19–22]. Accurate localization of static particles at high densities and low signal-to-noise ratio (SNR) has become feasible, and performance of localization algorithms as well as the required computational hardware will probably increase further.

[1]Institute for Microbiology and Biotechnology, Rheinische Friedrich-Wilhelms-Universität Bonn, Bonn, Germany. [2]Department of Physics, Carnegie Mellon University, Pittsburgh, PA, USA. [3]Laboratory of Biophysics, Wageningen University and Research, Wageningen, the Netherlands. [4]Microspectroscopy Research Facility, Wageningen University and Research, Wageningen, the Netherlands. ✉e-mail: KoenJAMartens@gmail.com

The second analysis step (tracking), however, is impeded by high computational complexity, especially when considering global information and taking possible state-changing, blinking and bleaching behavior into account[23–25]. Currently, most sptPALM experiments are designed to reduce this computational complexity by using a very low density of nonblinking particles (that is, <0.1 μm^{-2}) over long data acquisition times[2,23]. Even with these considerations, tracking algorithms require a priori parameters, such as the likelihood of state-changing or bleaching, maximum search radius and expected blinking behavior; still, the obtained trajectory information could unknowingly contain imperfect linkages. The resulting trajectories can additionally be deteriorated by spurious localizations, which is often unavoidable in live-cell imaging[26].

The trajectories are then quantitatively interpreted by, for example, analyzing jump distance (JD) histograms or mean squared displacement (MSD) curves. Multiple diffusional states can be extracted from the summation of individual trajectories: state-transitioning populations can be elucidated via for example diffusion distribution analysis (DDA)[9,27,28] or analysis by unsupervised Gibbs sampling (SMAUG)[29]; while nontransitioning populations can be elucidated via JD distributions (JDDs; for example, Spot-On[30]). Alternatively, individual trajectories can be classified in populations via analytical (for example, exTrack[24] or vbSPT[31]), statistical[32,33] or machine-learning[34] approaches, or quantitatively compared between experimental conditions[35]. However, not all of these methods fully utilize the information within a trajectory—for instance, a JD histogram analysis does not require information on the complete trajectory, only whether or not two localizations are linked together on consecutive frames. Additionally, trajectory interpretation is heavily, but unbeknownst, influenced by wrong trajectory information. Taken together, tracking algorithms do not take full advantage of recent developments in (high-density) particle localization, have high computational complexity and can unknowingly introduce linkage errors, and full trajectory information is not always utilized to obtain state-of-the-art biological knowledge.

In this Article, we propose an area-averaged analysis method that does not require a priori assumptions, cannot introduce linkage errors and is minimally influenced by localization density, particle blinking, and random or structured spurious localizations. Temporal analysis of relative distances (TARDIS) performs a global analysis on all relative spatiotemporal distances, inspired by methods that infer localization precision or structures from relative distances of particles[36–38], and provides information on the particle dynamics of a specific area, rather than on the single-trajectory level. TARDIS does not use any tracking algorithm and thus circumvents required inherit assumptions and experimental considerations. We show that TARDIS provides accurate quantitative measures and outperforms existing tracking algorithms in obtaining accurate JDDs in complex SPT conditions, such as high-density localization, heavily noise-deteriorated situations, blinking particles and undergoing intricate, non-Brownian, diffusive motion. TARDIS can accurately deduce unknown JDDs, analytically described single and double Brownian-motion populations in pure diffusion conditions, in confined diffusion or under flow; state-switching populations in pure diffusion conditions and in confined diffusion; and can be expanded to other analytically described conditions.

Our method to analyze tracking data will open the way for new experimental avenues by allowing higher particle densities, a wider pool of possible probes and lower impact of spurious background localizations. We focus on fluorescence sptPALM data throughout this manuscript, but note that TARDIS is method-agnostic and can be applied to all SPT data. We provide TARDIS as a ready-to-use software (Supplementary Software), both as a stand-alone graphical user interface (GUI) and as a MATLAB function for incorporation in analysis routines[39] (Supplementary Note 1).

Results

The TARDIS algorithm

Our proposed TARDIS method is a parameter-free algorithm that only requires spatiotemporal information of particle localizations (Fig. 1a). TARDIS connects all localizations on frame N to all localizations on frame $N + \tau$, where the temporal shift τ is gradually increased (Fig. 1a,b). TARDIS then collects the JDs, visualized here as a histogram. At small values of τ (that is, τ smaller or equal to the observed trajectory length of a particle), the linkages between localizations fall in two distinct categories: (1) linkages in which both localizations belong to the same particle (blue lines in Fig. 1b; intraparticle links) or (2) linkages in which the localizations do not belong to the same particle (red lines in Fig. 1b; interparticle links). Importantly, at large values of τ, that is, τ larger than the maximum trajectory length in the dataset, only interparticle links (red) will be obtained (Fig. 1b, right). The underlying interparticle links distribution is insensitive to time, that is, it does not vary over values of τ, but does depend on the spatial distribution of localizations within each individual experiment. We have derived this spatial distribution for exemplary model scenarios (Supplementary Note 2). The intraparticle links contained in the data obtained at small τ (Fig. 1b, bottom) can be extracted. Either the interparticle links distribution found at large τ (red curve) can be subtracted (called 'TARDIS-JD' from here on), or, ideally, it can be fitted with a combination of the interparticle links distribution along with an analytical distribution describing the intraparticle links (blue curves). This combined fitting routine is less sensitive to noise and provides more accurate fitting results compared to TARDIS-JD. Starting parameters for the full TARDIS routine can be estimated by first performing TARDIS-JD ('estimation fit'). Alternatively, TARDIS-JD extraction can be used independently to obtain JDDs for datasets that contain dynamics that have not yet been analytically described, such as complex multistate dynamics and/or directed motion, or obtained from unknown underlying dynamics. An in-depth description of the TARDIS software implementation is given in Supplementary Note 1.

Any analytical distribution that describes JDs over multiple τ values can generally be used in TARDIS. TARDIS includes analytical fitting of single and multiple populations of Brownian motion, diffusion under flow, confined diffusion, fast state-switching behavior (anaDDA[27]), and allows for user-defined analytical distributions (Supplementary Note 3). We employ a single-population, freely diffusive fit in Fig. 1. Additionally, the rate at which the intraparticle links fraction decreases as a function of τ can be used as a measure for bleaching kinetics (Supplementary Notes 2 and 4). Further, the value of τ at which only interparticle linkages are present can be estimated without a priori information via a one-sided Wilcoxon statistical test (which deduces the value of τ at which the JDDs do no longer change as a function of τ; Supplementary Note 5), which makes TARDIS an analysis method for particle dynamics that does not require any a priori parameters. Finally, TARDIS can provide the user with statistical estimates about particle parameters, such as mean JD, blinking probability and average trajectory length (Supplementary Note 6) The TARDIS software is available as open-source MATLAB code and as a stand-alone GUI program[39].

TARDIS outperforms existing SPT methods

Current state-of-the-art static localization algorithms can localize immobile particles with up to ~5 localizations μm^{-2} per frame densities[17,18], whereas current tracking algorithms normally operate at «0.1 localizations μm^{-2} per frame[2,23], indicating a big gap in accessible densities. Further factors complicating tracking algorithms are the blinking of (fluorescent) particles and the presence of localizations not belonging to trajectories. These can either arise from experimental properties (for example, photo-physics and autofluorescence), but also from faulty localization, especially when combining blurry, mobile point spread functions with multiparticle fitting (Discussion). To investigate the performance of TARDIS in these complex spt(PALM) conditions,

https://doi.org/10.1038/s41592-023-02149-7

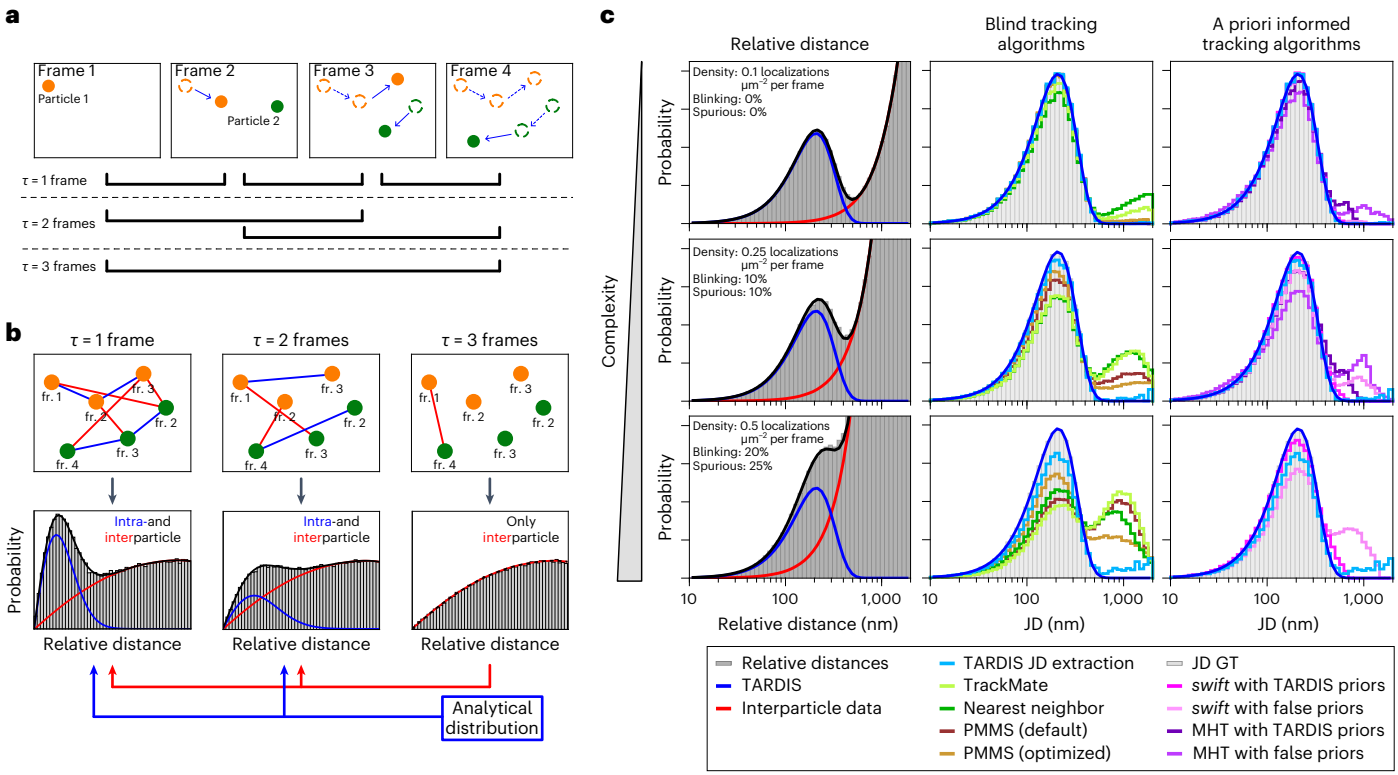

Fig. 1 | Overview of the TARDIS algorithm and comparison to tracking algorithms. a, To exemplify the TARDIS algorithm, two diffusing particles are simulated, starting on frame 1 and frame 2, respectively. The spatiotemporal positions of the localizations are recorded. TARDIS compares the positions on all frames with a set time shift τ, here illustrated for $\tau = 1$, 2 and 3 frames. **b**, All localizations at time t are compared to all localizations at multiple times $t + \tau$ over the complete temporal range, illustrated for $\tau = 1$, 2 and 3 frames. At τ smaller than the longest trajectory (that is, $\tau < 3$ frames in this example), the distribution that can be determined from the relative distances contains information from both intra- and interparticle links (blue and red lines, respectively). Using a temporal shift that is larger than the longest trajectory (that is, $\tau \geq 3$ frames in this simulated example), only interparticle links are present in the distribution (red lines). This interparticle links distribution is used in conjunction with an analytical distribution (a single population fit is shown here) to fit the distributions obtained from temporally analyzed relative distances. Distributions in **b** are created via a simulation of 25,000 particles. fr., frame. **c**, Comparison of TARDIS with SPT algorithms. Three simulated (20,000 trajectories) datasets (10 ms frame time) with increasing complexity (by increasing localization density, particle blinking and spurious localization density) are analyzed with TARDIS (left; $\tau = 1$ frame shown here) and compared to (middle) the blind tracking algorithms uTrack-inspired PMMS[40,42] (dark brown: default parameters; light brown: user-optimized parameters based on the known GT), TrackMate[40,41] (light green) and nearest neighbor analysis (dark green), and (right) to the prior-informed methods *swift* (Endesfelder et al., manuscript in preparation) (magenta) and MHT[25] (purple; MHT at the most complex dataset did not run to completion). These prior-informed methods are optimized via TARDIS output, specifically mean JD, bleaching lifetime, spurious localizations and trajectory density.

we simulated (Methods) datasets of particles with increasing particle density, particle blinking and spurious localization density, which all effectively increase the amount of interparticle linkages relative to intraparticle linkages, hereafter called 'complexity' (Fig. 1c, left, and Supplementary Note 7).

The simulated datasets were analyzed (Fig. 1c, also see Extended Data Fig. 1) with TARDIS (blue, cyan) and compared to the JD ground truth (GT: gray histogram), as well as to analysis with a range of tracking algorithms with a varying degree of inherit assumptions and a priori information.

First, we compared TARDIS to blind tracking algorithms (that is, tracking algorithms that do not rely on a priori information; Fig. 1c, middle column). The minimally informed nearest-neighbor tracking analysis (dark green) is robust at low complexity, but generates incorrect linkages at higher complexity. The linear assignment problem tracker embedded in TrackMate[40,41] (light green) performs a spatiotemporal global optimization protocol, and is especially optimized for Brownian motion. TrackMate provides similar results as nearest-neighbor tracking. Finally, PMMS[42] (piecewise-stationary motion model and iterative smoothing) is an algorithm that expands on uTrack[40] by fusing past and future information of individual potential trajectories optimized for heterogeneous motion, which excels at high-density tracking in the tracking challenge[23]. PMMS was optimized by manually changing parameters that do not describe diffusive behavior of the particles, but rather affect its computational complexity (dark brown, default settings; light brown, manually optimized settings). This manual optimization improves PMMS' results and outperforms the other tracking methods in these datasets, but does not fully describe the GT at medium or high complexity.

The comparison of TARDIS to a priori informed tracking algorithms (Fig. 1c, right column), showcases using TARDIS to provide priors on tracking parameters to assist these complex tracking algorithms (Supplementary Note 6). *swift* is a global Bayesian tracking method (Endesfelder et al., manuscript in preparation, beta-testing repository http://bit.ly/swifttracking, magenta), which relies on providing a priori estimations for the parameters and then determines the most probable solution. The multiple-hypothesis tracking[25] (MHT) algorithm, implemented in the Icy software[43], combines physics-inspired target particle existence models with realistic motion models in cellular environments.

TARDIS shows excellent agreement with the GT throughout the tested parameter space, also when only extracting the JDs (TARDIS-JD extraction, cyan in Fig. 1c) rather than fitting the population. *swift* and MHT improve when using meaningful a priori information, for example,

TARDIS-generated. Blind tracking algorithms behave adequately at low complexity, but show nonexisting high JD at increased complexity, due to incorrect interparticle linkages, which can be attributed to inherit 'greediness' of these tracking software to link localizations together, rather than terminating trajectories. We also observed under-estimation of JD via the tracking algorithms at high densities and high diffusion coefficients, which is a result from linking localizations from different particles together (Extended Data Fig. 2).

TARDIS is accurate on highly complex single-particle data

As the TARDIS algorithm performs well under complex scenarios, we investigated to what extent TARDIS remains accurate (also see Supplementary Note 8). We investigated (1) well-localized single-particle trajectories across a range of diffusion coefficients (with 10 ms frame time) and densities (Fig. 2a,d), (2) the influence of spurious noise and blinking particles ('localization inaccuracies') (Fig. 2b), (3) multiple diffusive populations combined with previously established complexity (Fig. 2c) and (4) effects of spatial heterogeneity in particle density or diffusivity (Supplementary Note 9).

We tested TARDIS' accuracy by analyzing simulated single-population diffusion with a varying degree of particle density and diffusion coefficient (Fig. 2a). The complexity increases throughout the tested parameter space, as indicated by the increasing ratio of intraparticle and interparticle links. TARDIS can accurately (<5% normalized root mean square error, nRMSE) compute single-population diffusion up to ~50× higher particle densities than commonly used in spt(PALM) (5 localizations μm^{-2} per frame), assuming localization is accurate at these high densities, with all tested varying diffusion coefficients (up to 10 $\mu m^2 s^{-1}$, localized every 10 ms) to further increase complexity (Fig. 2a; for comparison with tracking methods, see Extended Data Fig. 2; detailed fitting results are shown in Extended Data Fig. 3). We note that the nRMSE of the found diffusion parameter scales qualitatively with the complexity, indicative that TARDIS will still be accurate at even higher complexity (Supplementary Note 8).

Incorporating inaccurate localizations (that is, false positive (FP) or false negative (FN)) in our simulations (Fig. 2b) reveals the insensitivity of TARDIS to both FP (for example, spurious localizations) and missing true positives (TP; for example, blinking particles or particle moving temporarily out of focus). Diffusion coefficient (Extended Data Fig. 3) and bleach time (Extended Data Fig. 4) are accurately retrieved up to the condition where 50% of the localizations are removed (that is, on average ~1.5 localizations per particle or ~1.2 consecutive localizations per particle) while simultaneously 50% of the dataset consists of FP localizations. In fact, an ~10% nRMSE is still achieved when more than 99.9% of all information in the relative distance histograms is attributed to interparticle linkages (Extended Data Fig. 5).

Additionally, we investigated TARDIS' limits with respect to trajectory density, total trajectory count, spurious localization density and fluorophore blinking, based on TARDIS' mathematical foundation (Methods and Supplementary Notes 2 and 8). Our analysis revealed that TARDIS can retrieve a single, 1 $\mu m^2 s^{-1}$, diffusive population with ~3% uncertainty given 10,000 trajectories for anywhere between 0.1 and 10 trajectories starting each frame, or with <25% error with just 100 trajectories with 0.1–1 trajectories starting each frame (Supplementary Fig. 9a). Our analysis further showed that TARDIS' accuracy is either limited by trajectory density or spurious localization, but not both (Supplementary Fig. 9b), and that strongly blinking particles can, in certain cases, increase TARDIS' accuracy compared to nonblinking particles (Supplementary Fig. 9c). Finally, we showed that TARDIS' accuracy only improves with using more temporal shift (τ) bins when the bleach half-time is sufficiently large (Supplementary Fig. 9d).

Next, we investigated the accuracy of TARDIS in conditions with complex datasets, which additionally have two diffusive populations rather than one (Fig. 2c). TARDIS accurately fits the relative distance histogram with a mixture of interparticle distribution and two diffusive populations, whereas the JD histogram obtained via tracking algorithms does not clearly show the separate populations. JD extraction in TARDIS (cyan curve in Fig. 2c) does accurately show the JD GT.

Finally, we assessed TARDIS under experimental conditions with increased complexity (Fig. 2d and Extended Data Fig. 6). To do so, we imaged freely diffusing fluorescent ~100-nm-diameter beads in water, imaged with 200 µs stroboscopic illumination to minimize localization artifacts (Methods), while changing the bead density and frame time (that is, increasing JD). These datasets were localized and analyzed via TARDIS, TARDIS-JD extraction and nearest-neighbor tracking. At more complex scenarios, nearest-neighbor tracking and TARDIS-JD fail to accurately deduce JDs. Due to the global fitting nature of TARDIS (that is, over multiple values of τ), the diffusion coefficient can still be accurately extracted (lower panels in Fig. 2d). These results are very similar to the ones obtained via simulated trajectories or TARDIS' mathematical description (Supplementary Notes 2 and 8).

Combining these results indicate that TARDIS is largely unaffected by regularly encountered particle, sample or computational imperfections or influences that have a large impact on traditional sptPALM analysis accuracy. The scaling of TARDIS' accuracy with complexity clearly indicates that experimental data will be hindered by localization artifacts sooner than by inaccurate TARDIS analysis (Supplementary Note 8). Additionally, we investigated scenarios that could hypothetically bias TARDIS and discuss these in Supplementary Note 9. This investigation establishes that TARDIS bias is only introduced when the interparticle linkage histogram (red in Fig. 1) does contain information on intraparticle linkages (that is, TP trajectories). Bias of this kind can normally be circumvented by determining the τ at which intraparticle linkages are exclusively present via a statistical test (one-sided Wilcoxon, see Supplementary Note 5). Only if the experimental particle bleach time (also taking, for example, movement out of the field of view (FoV) or focus into account) is on the same order of magnitude as the experimental time, no proper interparticle linkage histogram can be created, and TARDIS will be biased.

Importantly, our investigations revealed that TARDIS cannot 'fail silently', that is, provide data that at glance look accurate, but contain errors: TARDIS failures due to wrong localization shows clear errors in the residuals of the fit (Supplementary Note 9). A recent computational method that performs an analysis similar to our TARDIS-JD extraction, but with interparticle data obtained from $\tau = 0$ frames, further emphasizes the robustness of our approach[44] (Extended Data Fig. 10).

TARDIS accurately elucidates intricate diffusive behavior

So far, we have focused on well-described single- or double-population Brownian motion. However, in biological conditions, this is normally not the case, and the diffusive behavior is more intricate. Therefore, we assessed how TARDIS handles diffusional complexity (Fig. 3 and Supplementary Note 3).

First, we analyzed simulated datasets provided as part of a comparison of particle tracking methods[23] (Fig. 3a and Extended Data Fig. 7). Since the underlying biological model changes throughout the datasets, we used the TARDIS-JD extraction. To investigate the effect of data complexity, we reshuffled the 'Receptors' trajectory localizations (described as 'tethered motion, switching, any direction') to obtain a high density of particles (380 particles per frame or ~0.15 localizations μm^{-2}). Additionally, we removed localizations according to the four SNR levels (SNR of 7, 4, 3 and 1, equivalent to removing 0%, 24%, 54% and 85% of localizations, assuming perfect localization at SNR of 7, and scaling logarithmically) used in the comparison[23]. While the JD histograms show intricate behavior over a range of temporal shifts, TARDIS-JD extraction shows good agreement with the GT for the SNR of 7, 4 and 3 levels (Fig. 3a). The other simulated datasets from this resource were also analyzed in this way (Extended Data Fig. 7), showcasing that TARDIS-JD extraction can handle challenging datasets with intricate diffusive behavior. Additionally, TARDIS is able to analytically

https://doi.org/10.1038/s41592-023-02149-7

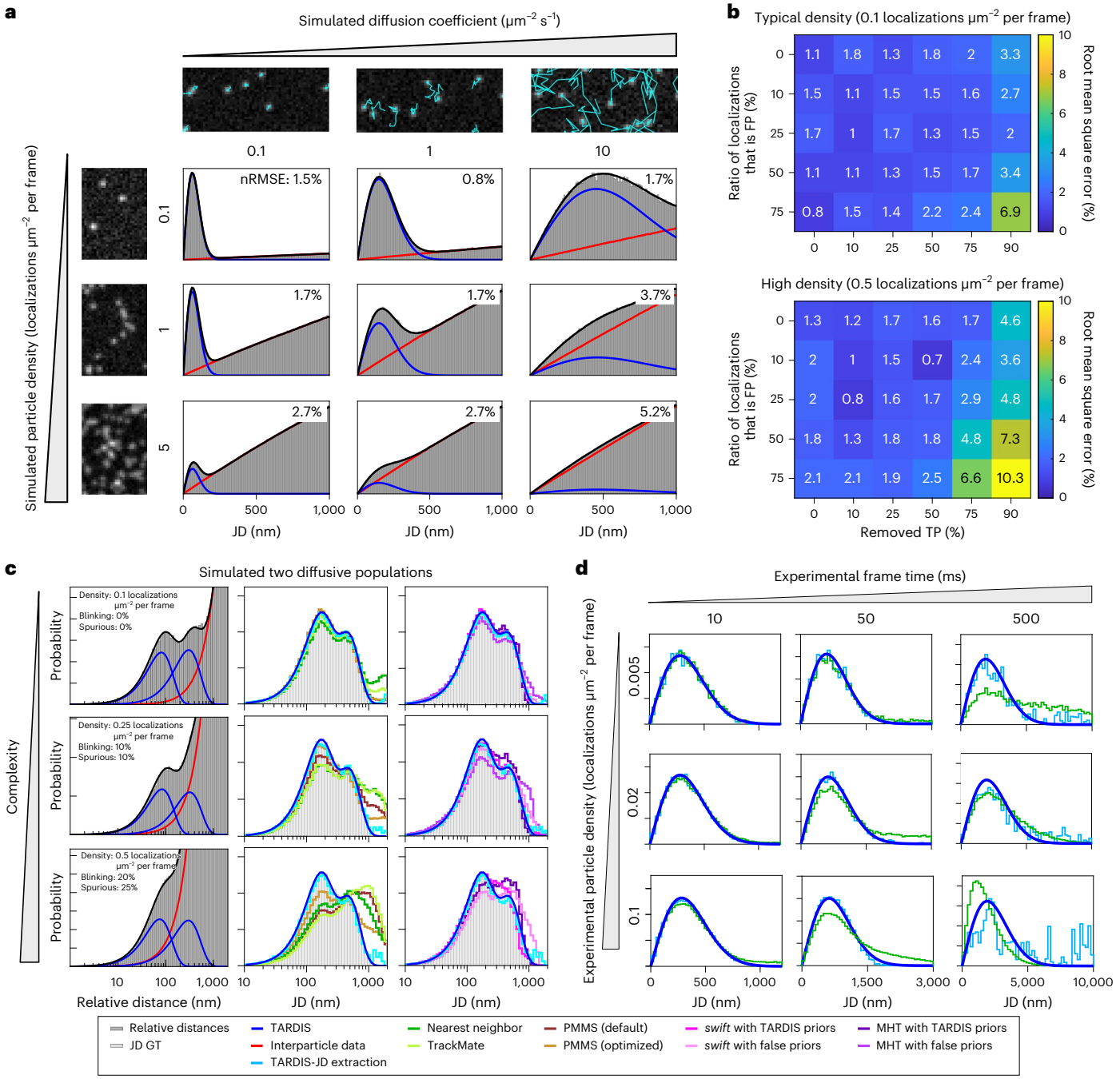

Fig. 2 | Performance of TARDIS in complex conditions. a, Visualization of a TARDIS fit across a range of particle densities (vertical) and diffusion coefficients (horizontal). TARDIS is performed on 20,000 simulated localizations with 30 nm localization precision; images on the left show representative particle density, images on the top show representative JDs (over 20 frames) in cyan. These data were fitted via TARDIS with a single-population Brownian motion fit. The simulations and TARDIS fits were repeated ten times, and the normalized root mean square error (nRMSE; normalized to diffusion coefficient) from these iterations is reported in the top right of every subplot. Detailed information and comparison with tracking algorithms can be found in Extended Data Figs. 2 and 3. **b**, Error of the TARDIS fit of a single diffusive population (bleaching half-time of three frames) at different particle densities and different levels of localization inaccuracy. Simulations of particle trajectories with a diffusion coefficient at 1 $\mu m^2 s^{-1}$ at densities of 0.1 and 0.5 localizations μm^{-2} per frame were degraded by randomly removing TP localizations from the trajectories and/or adding unstructured FP localizations randomly throughout the FoV in various contributions. Reported values are calculated from ten repetitions of every condition. Detailed information can be found in Extended Data Figs. 3 and 4. **c**, Fitting two populations in TARDIS scales similarly with complexity. Trajectories were simulated and analyzed with identical parameters as specified in Fig. 1b, except half the trajectories were given a 0.5 $\mu m^2 s^{-1}$ diffusion coefficient, and the other half a 5 $\mu m^2 s^{-1}$ diffusion coefficient—and analysis with TARDIS was performed with two populations. The information is also presented on a linear *x* axis in Extended Data Fig. 1. **d**, Experimental single-particle mobility assessed by TARDIS compared to TARDIS-JD and nearest-neighbor tracking in a range of complexities by increasing the fluorophore concentration and increasing the frame time while keeping excitation time constant. To fully prevent multiparticle artifacts (Supplementary Note 9), the localization list belonging to the highest density is created via the localizations of the lowest density. Throughout this parameter space, the same total experiment time was used (250 s).

https://doi.org/10.1038/s41592-023-02149-7

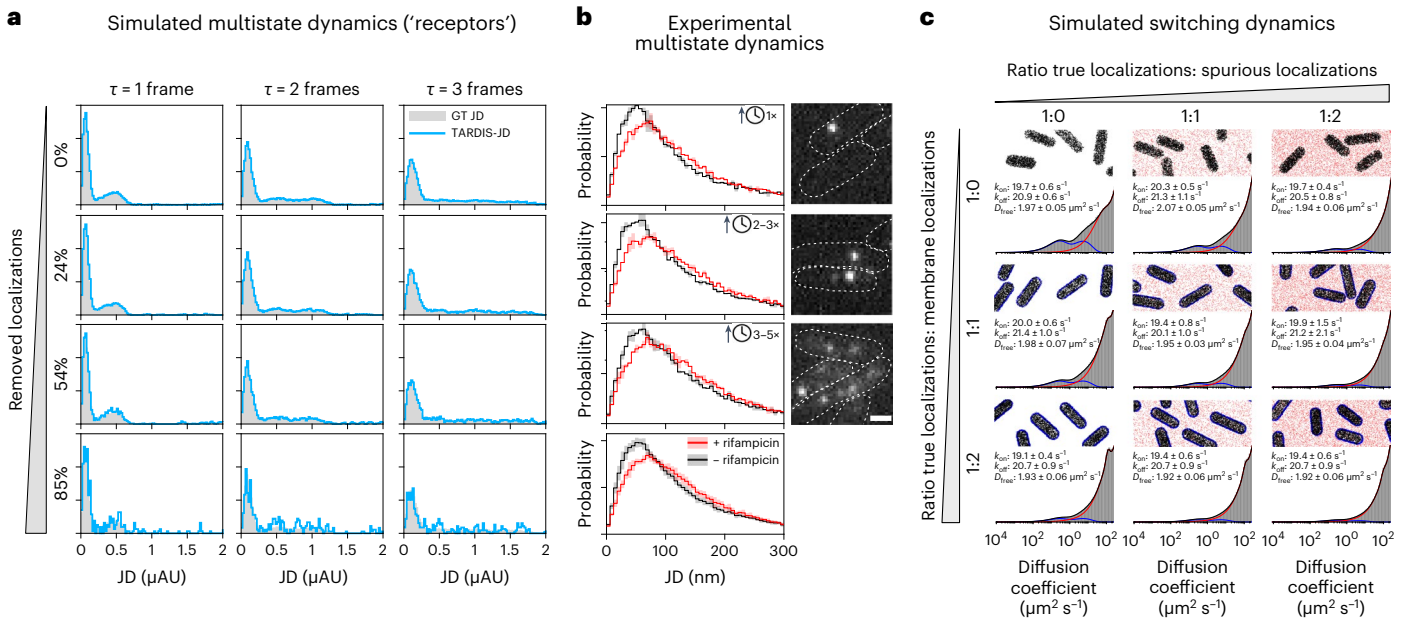

Fig. 3 | TARDIS enables high-complexity single-particle mobility experiments of intricate diffusive behavior. a, The 'Receptors' tracking data from Chenouard et al.[23] (localization density set at 0.15 localizations μm^{-2} per frame) has been deteriorated by removing localizations to simulate lower signal-to-noise conditions similar to Chenouard et al.[23] (rows) and analyzed via TARDIS-JD extraction, and compared to the GT data. The complex diffusive behavior of these particles cannot be well described analytically, as the JD histograms over time shifts (columns) show. The following TARDIS settings were used: τ bins of one to three frames; maximum JD of 10 μAU (micro-arbitrary units as introduced by Chenouard et al.[23]). Other simulated datasets from this resource can be found in Extended Data Fig. 7. **b**, JD analysis of RNA polymerase in *E. coli* with (red) and without (black) rifampicin. By increasing the photo-conversion rate, the total time required to obtain 80 localizations μm^{-2} (within cells) is decreased by a factor of ~2.5 (second panel), then by a factor ~4 (third panel). Insets on the right show exemplary frames of these movies. The bottom panel combines the JD histograms of the top three panels. Lines indicate average of two biological replicates; shaded area indicates the standard deviation. Scale bar, 1 μm. **c**, Fitting of a simulated state-changing population in bacterial cells (k_{on}, k_{off} = 20 s^{-1}, D_{free} = 2 μm^2 s^{-1}, three frame bleaching half-time, with trajectory length capped at eight frames). Inaccuracies from GT are introduced as spurious localizations (columns, red localizations) and membrane-bound localizations (rows, blue localizations). Reported values are median ± quartile determined from ten repetitions. Detailed information about the TARDIS fits can be found in Extended Data Fig. 9. Simulation datasets consist of 10,000 'TP' trajectories at 10 ms frame time.

extract diffusion coefficients under conditions of flow or confined diffusion (Supplementary Note 3), and we note that TARDIS can be expanded with any analytical description of JDDs, analogous to our implementation of these two examples.

Next, we explored the use of TARDIS to reduce imaging time in sptPALM, which is beneficial to minimize the effects of temporally changing physiology, either biological or for example due to phototoxicity. RNA polymerase (RNAP) in *Escherichia coli* has dynamic diffusive behavior that does not satisfy a known analytical model[45,46]. Rifampicin is a transcription inhibitor that decreases the promoter search and transcription kinetics, effectively increasing the diffusivity of RNAP[45,46]. Therefore, we used TARDIS-JD extraction and qualitatively assess the obtained JD histograms (Fig. 3b). By increasing the primed conversion efficiency (that is, increasing 488 nm laser power) in repetitions of the experiment[47,48], we were able to reach the same total number of localizations per cell area (80 localizations per 1 μm^2 cell area) much faster, decreasing the total experiment time step-wise ~2–3-fold and ~3–5-fold (both compared to the top panel). Addition of rifampicin is characterized by a shift toward higher RNAP JDs, which is clearly observed after TARDIS-JD extraction (Fig. 3b). Even though the change in JD is only ~30 nm, this small difference is consequently extracted via both low- and high-throughput sptPALM-TARDIS (Fig. 3b, bottom), which is not the case when assessing this data via nearest-neighbor tracking (Extended Data Fig. 8). A further decrease of imaging time is hindered not by TARDIS, but rather by difficulties in the localization procedure, for example, fitting overlapping, blurry point-spread functions (PSFs) (Discussion).

Finally, we investigated a scenario in which state-switching sptPALM in prokaryotic cells is simulated. First, we note that confinement in cells strongly influences the obtained diffusion coefficient, which can be corrected with TARDIS (Supplementary Note 3). In our simulations, the trajectories show transient binding with specific kinetics that can be extracted with DDA approaches[9,27,28], after a translation from JD to apparent diffusion coefficient. The simulated data is deteriorated by spurious localizations on the cell membrane (structured noise), and additionally randomly throughout the FoV (unstructured noise) (Fig. 3c and Extended Data Fig. 9). The GT simulation parameters are recovered via TARDIS with small (<5%) error with respect to using analytical DDA on the GT trajectories throughout the tested deterioration, even in the extreme case in which the ratio of TP:spurious localizations:membrane localizations is 1:2:2 (that is, only 20% of localizations are GT trajectory information).

These experiments showcase that TARDIS enables measurements in experimental conditions that are currently largely inaccessible via tracking-based analysis, removing the current stringent metrics such as low-density, long-duration experiments and nonblinking particles (also see Supplementary Note 8). TARDIS opens up the opportunity to obtain high-statistical diffusion information in shorter time, which in turn decreases the inherently present temporal averaging in single-particle experiments.

Discussion

SPT analysis is limited by both computational complexity and stringent experimental requirements. Reconstructing truthful particle trajectories from a dataset with spatiotemporally close trajectories is challenging without accurate a priori information, and is even further complicated by the blinking and/or fast bleaching of particles. TARDIS solves all these issues by analyzing all-to-all particle distances over

multiple temporal shifts. TARDIS accurately resolves single, double and state-changing populations in challenging conditions, outperforming existing SPT algorithms. Finally, we show that traditional sptPALM experiments can be performed up to 5× faster without loss of information with current localization methods. Faster data acquisition is especially useful in biological conditions where a short event needs to be investigated, such as recovery from DNA damage, or protein organization during, for example, phage infection or cell division. TARDIS is provided as an easy-to-use software tool via a GUI or implementable script-wise[39] (Supplementary Software).

TARDIS is robust with respect to all causes that increase SPT complexity: (1) high density of trajectories, (2) blinking particles or short trajectories, (3) unstructured spurious localizations and (4) structured spurious localizations. We thoroughly investigate TARDIS' limits in this respect via its mathematical foundation (Supplementary Notes 2 and 8). Furthermore, TARDIS is agnostic to the type of particle movement (that is, non-Brownian motion), requires a low number of trajectories to obtain satisfactory fit outcomes (Supplementary Note 8) and can use any analytical description of JDDs (Supplementary Note 3). We believe that the high robustness of TARDIS is especially useful in sptPALM where the dynamics and localization are coupled, and a high local density influences the perceived dynamics.

TARDIS provides area-averaged information about particle dynamics rather than trajectory-specific information. This can be performed for the whole FoV as showcased so far, but can also be performed in a sub-FoV manner to spatially assess the distribution of multiple or mixed populations with ~250 nm resolution or lower (Supplementary Note 10). TARDIS can be used on its own, or alternatively, the output of TARDIS can be used as accurate a priori information in tracking software, especially Bayesian SPT software (for example, *swift*, MHT[25] or others[49,50]). Via this combination (Figs. 1c and 2c), accurate tracking is ensured while full trajectory information is extracted. Quantitative parameter extraction on particle mobility via TARDIS requires analytical descriptions of JDDs, and thus TARDIS is limited by the existence of these models. Additionally, it conceptually hinders the incorporation of an individual trajectory's past and future information within the fitting models. TARDIS as presented here only assesses two-dimensional localization data, but it can be expanded to investigate three-dimensional data or perform separate analytical fitting routines on separate spatial dimensions.

We show that with the introduction of TARDIS, and especially combined with *swift* or MHT, the new limitation for high-throughput sptPALM analysis is high-density localization of mobile particles. Current localization implementations specifically designed for high-density datasets focus on immobile particles, which introduces two artifacts when using on datasets of mobile particles: (1) motion-blurred localizations are often interpreted as multiple static particles, and (2) information on multiple frames is included, which collapses localizations of close-by particles on consecutive frames to the same location, rather than accurately deducing a small JD. Artifact 1 can be remedied via stroboscopic illumination[51], but this cannot always be implemented due to hardware limitations and light dose considerations on live cell health. Artifact 2 shows the clear need for high-density localization algorithms optimized for mobile particles. Throughout this manuscript, we show that TARDIS is unaffected by densities of about an order of magnitude higher than can currently be accurately extracted from current state-of-the-art localization algorithms that can handle densities up to 5 localizations μm^{-2}(refs. 17,18).

In conclusion, TARDIS is a software platform that negates all traditionally avoided circumstances in spt(PALM), such as high-density or strongly blinking particles. TARDIS therefore opens up the possibility of performing data analysis on mobile particles with paradigm-shifting conditions and enables the exploration of novel experimental designs.

Online content

Any methods, additional references, Nature Portfolio reporting summaries, source data, extended data, supplementary information, acknowledgements, peer review information; details of author contributions and competing interests; and statements of data and code availability are available at https://doi.org/10.1038/s41592-023-02149-7.

References

1. Elf, J. & Barkefors, I. Single-molecule kinetics in living cells. *Annu. Rev. Biochem.* **88**, 635–659 (2019).
2. Shen, H. et al. Single particle tracking: from theory to biophysical applications. *Chem. Rev.* **117**, 7331–7376 (2017).
3. Martens, K., van Duynhoven, J. & Hohlbein, J. Spatiotemporal heterogeneity of κ-carrageenan gels investigated via single-particle-tracking fluorescence microscopy. *Langmuir* **20**, 5502–5509 (2020).
4. Prigent, S., Valades-Cruz, C. A., Leconte, L., Salamero, J. & Kervrann, C. STracking: a free and open-source Python library for particle tracking and analysis. *Bioinformatics* **38**, 3671–3673 (2022).
5. Sbalzarini, I. F. & Koumoutsakos, P. Feature point tracking and trajectory analysis for video imaging in cell biology. *J. Struct. Biol.* **151**, 182–195 (2005).
6. Manley, S. et al. High-density mapping of single-molecule trajectories with photoactivated localization microscopy. *Nat. Methods* **5**, 155–157 (2008).
7. Ortega-Arroyo, J. & Kukura, P. Interferometric scattering microscopy (iSCAT): new frontiers in ultrafast and ultrasensitive optical microscopy. *Phys. Chem. Chem. Phys.* **14**, 15625–15636 (2012).
8. Kukura, P. et al. High-speed nanoscopic tracking of the position and orientation of a single virus. *Nat. Methods* **6**, 923–927 (2009).
9. Martens, K. J. A. et al. Visualisation of dCas9 target search in vivo using an open-microscopy framework. *Nat. Commun.* **10**, 3552 (2019).
10. Ohana, R. F. et al. HaloTag7: a genetically engineered tag that enhances bacterial expression of soluble proteins and improves protein purification. *Protein Expr. Purif.* **68**, 110–120 (2009).
11. Klein, T. et al. Live-cell dSTORM with SNAP-tag fusion proteins. *Nat. Methods* **8**, 7–9 (2011).
12. Stallinga, S. & Rieger, B. Accuracy of the Gaussian point spread function model in 2D localization microscopy. *Opt. Express* **18**, 24461–24476 (2010).
13. Li, Y. et al. Real-time 3D single-molecule localization using experimental point spread functions. *Nat. Methods* **15**, 367–369 (2018).
14. Xu, F. et al. Three-dimensional nanoscopy of whole cells and tissues with in situ point spread function retrieval. *Nat. Methods* **17**, 531–540 (2020).
15. Aristov, A., Lelandais, B., Rensen, E. & Zimmer, C. ZOLA-3D allows flexible 3D localization microscopy over an adjustable axial range. *Nat. Commun.* **9**, 2409 (2018).
16. Nehme, E., Weiss, L. E., Michaeli, T. & Shechtman, Y. Deep-STORM: super-resolution single-molecule microscopy by deep learning. *Optica* **5**, 458–464 (2018).
17. Speiser, A. et al. Deep learning enables fast and dense single-molecule localization with high accuracy. *Nat. Methods* **18**, 1082–1090 (2021).
18. Nehme, E. et al. DeepSTORM3D: dense 3D localization microscopy and PSF design by deep learning. *Nat. Methods* **17.7**, 734–740 (2020).
19. Li, N. et al. Photonic resonator interferometric scattering microscopy. *Nat. Commun.* **12**, 1744 (2021).
20. Cnossen, J. et al. Localization microscopy at doubled precision with patterned illumination. *Nat. Methods* **17**, 59–63 (2020).

21. Jouchet, P. et al. Nanometric axial localization of single fluorescent molecules with modulated excitation. *Nat. Photonics* https://doi.org/10.1038/s41566-020-00749-9 (2021).
22. Gu, L. et al. Molecular resolution imaging by repetitive optical selective exposure. *Nat. Methods* **16**, 1114–1118 (2019).
23. Chenouard, N. et al. Objective comparison of particle tracking methods. *Nat. Methods* **11**, 281–289 (2014).
24. Simon, F., Tinevez, J.-Y. & Teeffelen, S. van. ExTrack characterizes transition kinetics and diffusion in noisy single-particle tracks. J. Cell Biol. https://doi.org/10.1083/jcb.202208059; https://doi.org/10.1101/2022.07.13.499913 (2022).
25. Chenouard, N., Bloch, I. & Olivo-Marin, J.-C. Multiple hypothesis tracking for cluttered biological image sequences. *IEEE Trans. Pattern Anal. Mach. Intell.* **35**, 2736–3750 (2013).
26. Floc'h, K. et al. Bacterial cell wall nanoimaging by autoblinking microscopy. *Sci. Rep.* **8**, 14038 (2018).
27. Vink, J. N. A., Brouns, S. J. J. & Hohlbein, J. Extracting transition rates in particle tracking using analytical diffusion distribution analysis. *Biophys. J.* **119**, 1970–1983 (2020).
28. Vink, J. N. A. et al. Direct visualization of native CRISPR target search in live bacteria reveals cascade DNA surveillance mechanism. *Mol. Cell* **77**, 39–50.e10 (2020).
29. Karslake, J. D. et al. SMAUG: analyzing single-molecule tracks with nonparametric Bayesian statistics. *Methods* **193**, 16–26 (2021).
30. Hansen, A. S. et al. Robust model-based analysis of single-particle tracking experiments with Spot-On. *eLife* **7**, e33125 (2018).
31. Persson, F., Lindén, M., Unoson, C. & Elf, J. Extracting intracellular diffusive states and transition rates from single-molecule tracking data. *Nat. Methods* **10**, 265–269 (2013).
32. Briane, V., Kervrann, C. & Vimond, M. Statistical analysis of particle trajectories in living cells. *Phys. Rev. E* **97**, 062121 (2018).
33. Momboisse, F. et al. Tracking receptor motions at the plasma membrane reveals distinct effects of ligands on CCR5 dynamics depending on its dimerization status. *eLife* **11**, e76281 (2022).
34. Granik, N. et al. Single-particle diffusion characterization by deep learning. *Biophys. J.* **117**, 185–192 (2019).
35. Pécot, T., Zengzhen, L., Boulanger, J., Salamero, J. & Kervrann, C. A quantitative approach for analyzing the spatio-temporal distribution of 3D intracellular events in fluorescence microscopy. *eLife* **7**, e32311 (2018).
36. Curd, A. P. et al. Nanoscale pattern extraction from relative positions of sparse 3D localizations. *Nano Lett.* **21**, 1213–1220 (2021).
37. Endesfelder, U., Malkusch, S., Fricke, F. & Heilemann, M. A simple method to estimate the average localization precision of a single-molecule localization microscopy experiment. *Histochem. Cell Biol.* **141**, 629–638 (2014).
38. Bohrer, C. H. et al. A pairwise distance distribution correction (DDC) algorithm to eliminate blinking-caused artifacts in SMLM. *Nat. Methods* **18**, 669–677 (2021).
39. TARDIS-public. *GitHub* (accessed 2023); https://github.com/kjamartens/TARDIS-public
40. Jaqaman, K. et al. Robust single-particle tracking in live-cell time-lapse sequences. *Nat. Methods* **5**, 695–702 (2008).
41. Tinevez, J.-Y. et al. TrackMate: an open and extensible platform for single-particle tracking. *Methods* **115**, 80–90 (2017).
42. Roudot, P., Ding, L., Jaqaman, K., Kervrann, C. & Danuser, G. Piecewise-stationary motion modeling and iterative smoothing to track heterogeneous particle motions in dense environments. *IEEE Trans. Image Process.* **26**, 5395–5410 (2017).
43. de Chaumont, F. et al. Icy: an open bioimage informatics platform for extended reproducible research. *Nat. Methods* **9**, 690–696 (2012).
44. Wolf, A., Volz-Rakebrand, P., Balke, J. & Alexiev, U. Diffusion analysis of nanoscopic ensembles: a tracking-free diffusivity analysis for nanoscopic ensembles in biological samples and nanotechnology. *Small* **19**, 2206722 (2023).
45. Bettridge, K., Harris, F. E., Yehya, N. & Xiao, J. RNAP promoter search and transcription kinetics in live E. coli cells. *J. Phys. Chem. B* **127**, 3816–3828 (2023).
46. Endesfelder, U. et al. Multiscale spatial organization of RNA polymerase in *Escherichia coli*. *Biophys. J.* **105**, 172–181 (2013).
47. Virant, D., Turkowyd, B., Balinovic, A. & Endesfelder, U. Combining primed photoconversion and UV-photoactivation for aberration-free, live-cell compliant multi-color single-molecule localization microscopy imaging. *Int. J. Mol. Sci.* **18**, 1524 (2017).
48. Turkowyd, B. et al. A general mechanism of photoconversion of green-to-red fluorescent proteins based on blue and infrared light reduces phototoxicity in live-cell single-molecule imaging. *Angew. Chem. Int. Ed.* **56**, 11634–11639 (2017).
49. Smal, I. et al. Multiple object tracking in molecular bioimaging by Rao-Blackwellized marginal particle filtering. *Med. Image Anal.* **12**, 764–777 (2008).
50. Ritter, C. et al. Data fusion and smoothing for probabilistic tracking of viral structures in fluorescence microscopy images. *Med. Image Anal.* **73**, 102168 (2021).
51. Elf, J., Li, G.-W. & Xie, X. S. Probing transcription factor dynamics at the single-molecule level in a living cell. *Science* **316**, 1191–1194 (2007).

Methods

Mathematical foundation of TARDIS

Fundamentally, TARDIS is a model-free analysis method that does not require a priori information on the intraparticle and interparticle distributions. However, for given scenarios, one can derive analytical descriptions of the distributions. To benchmark performance of TARDIS, we here describe the following scenario: a spatially random population with a single diffusive state is imaged in a square FoV. We here describe the distributions and contributions of the intra- and interparticle distributions (also see Supplementary Note 2).

The intraparticle probability density function (pdf) is governed by[52]

$$\mathrm{pdf}(\mathrm{JD}) = \frac{\mathrm{JD} \times e^{\frac{-\mathrm{JD}^2}{2\times\dim\times\left(D+\frac{\sigma^2}{\Delta t\times\tau}\right)\times\Delta t\times\tau-2\times\left(\frac{1}{6}\times\frac{\Delta t_{il}}{\Delta t}\right)\left(D+\frac{\sigma^2}{\Delta t\times\tau}\right)\times\Delta t\times\tau}}}{\dim\times\left(D+\frac{\sigma^2}{\Delta t\times\tau}\right)\times \mathrm{d}t\times\tau-2\times\left(\frac{1}{6}\times\frac{st}{\Delta t}\right)\left(D+\frac{\sigma^2}{\Delta t\times\tau}\right)\times \mathrm{d}t\times\tau} \quad (1)$$

In which JD is the jump distance (in m), dim is the dimensionality of the system, D the diffusion coefficient (in m s^{-2}), σ the localization uncertainty (in m), Δt the frame time (in s), Δt_{il} the illumination time (in s; assuming that the illumination pulse is an equidistant single-pulse sequence in each frame) and τ the temporal shift (in frames). We performed our benchmarking for dim of 2.

The interparticle probability density function in a two-dimensional square FoV is governed by[53]

$$g(s) = \begin{cases} 2d\left(-4\times\sqrt{d^2}+\pi+d^2\right) & 0 < d^2 \le 1 \\ 2d\left(-2+4\times\sin^{-1}\left(\frac{1}{\sqrt{d^2}}\right)+4\times\sqrt{d^2-1}-\pi-d^2\right) & 1 < d^2 \le \sqrt{2} \end{cases} \quad (2)$$

In which d^2 is the squared distance between two random points in a 1-by-1 arbitrary unit (AU) FoV.

The number of intraparticle distances found for temporal shift τ (in frames) on every frame f is governed by

$$n^{f,\tau}_{\text{intraparticle distances}} = \frac{2^{\frac{1-\tau}{\lambda_{\text{bleach}}}}}{2^{\frac{1}{\lambda_{\text{bleach}}}}-1} \times \frac{\lambda_{\text{bright}}\times\left(\lambda_{\text{dark}}\times 2^{\frac{-\tau}{\lambda_{\text{dark}}}+\frac{-\tau}{\lambda_{\text{bright}}}}+\lambda_{\text{bright}}\right)}{\left(\lambda_{\text{dark}}+\lambda_{\text{bright}}\right)^2} \times \left(1-p_{\text{nonlocalized}}\right)^2 \quad (3)$$

In which λ_{bleach} is the bleaching half-time of a particle (in frames), λ_{dark} and λ_{bright} the dark-state ('off') and bright-state ('on') half-times of the particle (in frames), and $p_{\text{nonlocalized}}$ the chance that a localization is not computationally recognized as such.

The number of interparticle distances found for temporal shift τ (in frames) on every frame f is governed by

$$n^{f,\tau}_{\text{interparticle distances}} = \left(\left(\frac{2^{\frac{1}{\lambda_{\text{bleach}}}}}{\left(2^{\frac{1}{\lambda_{\text{bleach}}}}-1\right)} \times d_{\text{traj}} \times \frac{\lambda_{\text{bright}}}{\lambda_{\text{dark}}+\lambda_{\text{bright}}} + d_{\text{spurious}}\right)\times\left(1-p_{\text{nonlocalized}}\right)\right)^2 - \left(\frac{2^{\frac{1-\tau}{\lambda_{\text{bleach}}}}}{2^{\frac{1}{\lambda_{\text{bleach}}}}-1} \times \frac{\lambda_{\text{bright}}\times\left(\lambda_{\text{dark}}\times 2^{-\frac{\tau}{\lambda_{\text{dark}}+\lambda_{\text{bright}}}}+\lambda_{\text{bright}}\right)}{\left(\lambda_{\text{dark}}+\lambda_{\text{bright}}\right)^2} \times \left(1-p_{\text{nonlocalized}}\right)^2\right) \quad (4)$$

In which λ_{bleach} is the bleaching half-time of a particle (in frames), d_{traj} the number of trajectories starting each frame, λ_{dark} and λ_{bright} the dark-state ('off') and bright-state ('on') half-times of the particle (in frames), d_{spurious} the number of spurious localizations per frame, and $p_{\text{nonlocalized}}$ the chance that a localization is not recognized as such.

The full TARDIS distribution over all temporal shifts τ can be derived from these equations, by calculating the ratio of intra- to interparticle distances via equations (3) and (4), and plotting the probability density functions set out in equations (1) and (2) according to this ratio. A full overview of the derivations for this foundation is provided in Supplementary Note 2.

Simulation of single and dual diffusive species

A redundant number of trajectories with an underlying specified diffusion coefficient and 30 nm localization precision (ignoring effects from motion blur) were simulated in a two-dimensional plane. The trajectories had a length determined via a three-frame half-life, with a frame time of 10 ms, on a FoV of 10 × 10 µm. To simulate blinking particles (where indicated), localizations were randomly removed from these trajectories. This localization list was then limited to the number of localizations that corresponds to 10,000 unfiltered trajectories. The trajectories were given a random starting frame, where the number of frames was varied to create a certain localization density. Then, spurious localizations were added, the amounts of which were based on the specified values and the number of localizations in the trajectories. These spurious localizations were randomly spread throughout the FoV and frames. For testing TARDIS with two diffusive populations, the same procedure was used, but all trajectories were randomly sampled from one of two populations with corresponding diffusion coefficients.

TARDIS was run on these datasets with the following settings (see Supplementary Note 1 for a full explanation of these parameters): maximum JD of 5 µm, maximum temporal shift (τ) of 3 frames, 10 frames longest trajectory length (determined via the Wilcoxon test), integration of 50 frames used for higher background subtraction accuracy, 30 nm localization precision, diffusion coefficient start value random between 0.1 and 10 µm^2 s^{-1}, using an estimation fit.

Simulation of state-switching species

For all specified conditions in the state-switching species (spurious and membrane localizations in 1:0, 1:0.5 and 1:1 ratio with respect to true localizations), ten repetitions of a simulation similar to ones described previously with the software encompassed in anaDDA[9,27,28] were created with the following settings: 40 (bacterial) cells (simulated as cylinders with length random between 2 µm and 3 µm and radius random between 0.45 µm and 0.55 µm, capped by two half-spheres with a radius identical to the cylinder radius; the cells were rotated and translated randomly throughout a 25 × 25 µm FoV) were populated with 300–500 particles in 2,000 frames (10 ms frame time). Trajectory lengths were pulled randomly from a decay with half-life of three frames (limited at eight frames). Localizations that were outside the FoV were discarded. Every particle was simulated with k_{on} = 50 s^{-1} or 20 s^{-1}, k_{off} = 30 s^{-1} or 20 s^{-1}, and D_{free} = 2 µm^2 s^{-1}, and localizations were subject to a 30 nm localization error. Simulation was performed with the software encompassed in anaDDA[27], in which a $1\cdot10^{-8}$ s steptime and a precision factor of 50000 was used. Starting frames for trajectories were randomly assigned. Spurious localizations were added where needed on the basis of the number of true localizations, and positioned randomly throughout the FoV. Membrane localizations were added where needed on the basis of the number of true localizations, and positioned in a two-dimensional, 100-nm-diameter slice at the simulated cell outlines.

All datasets were analyzed with TARDIS using the following settings (see Supplementary Note 1 for a full explanation of these parameters): anaDDA fit model with 0.5 µm radius, 3 µm length, 10 ms frame time and 30 nm localization precision. Maximum JD calculated was 2.5 µm (that is, average cell length), maximum Δt was 5 frames, 87 frames for longest trajectory length (determined via the Wilcoxon test) using the integration of 50 frames for higher background subtraction accuracy. anaDDA starting parameters were randomly chosen from 10–80 s^{-1}, 10–80 s^{-1} and 1–4 µm^2 s^{-1}, and an estimation fit (that is, a fit on remaining JDs after subtraction of interparticle fraction; Supplementary Note 1) was performed.

sptPALM microscopy

All microscopy was performed on home-build microscopes as described in detail elsewhere[54] that allows for imaging of Dendra2 proteins via primed conversion[48]. Briefly, live-cell experiments were performed on the following system: 561 nm (OBIS, Coherent), 488 nm (Sapphire LP, Coherent) and 730 nm (OBIS, Coherent) were combined and controlled via an acousto-optical tuneable filter (except the 730 nm laser) (AOTF; TF525-250-6-3-GH18, Gooch and Housego). The lasers were directed toward the back port of a Nikon Ti Eclipse microscopy body, and focused on the back-focal plane of a CFI Apo TIRF 100× objective (numerical aperture (NA) 1.49, Nikon) in HiLo mode via an ET DAPI/FITC/cy3 dichroic), and emission light passed through a ZT405/488/561rpc rejection filter and ET610/75 bandpass (all AHF Analysentechnik). The emission light was focused on an iXON Ultra 888 EMCCD camera (Andor) with an effective pixel size of 128 nm. The image acquisition was controlled by micromanager[55].

Bead experiments were performed on a similar microscope setup: a 638 nm laser line (Novanta) was controlled via a TriggerScope 4 (Advanced Research Consulting) connected to PycroManager[56], and directed toward the back port of the Nikon Ti body via a laser-coupled fiber (150 µm core diameter, Thorlabs). The laser light was directed via a reflective collimator and via a ZT405/488/561/642rpc and ZET405/488/561/642m-TRF dichroic/rejection filter combination (Chroma) to the back-focal plane of a 60× Apochromat TIRF 1.49 NA objective (Nikon) in HiLo mode. Emission light was passed through a 655-nm-longpass filter (655 LP ET, AHF Analysentechnik) and collected on a Prime BSI sCMOS camera (Teledyne Photometrics; 107 nm effective pixel size).

For the experiments on diffusive beads, carboxylate-modified FluoroSpheres (715/755 nm excitation/emission peaks, 97 nm diameter according to manufacturer) (Invitrogen, Thermo Fisher), were diluted 2,500 times or 10,000 times in purified water. After 5 min sonication, these solutions were placed in an Ibidi eight-chamber-well slide (Ibidi), and imaging was performed in a temperature-controlled (20 ± 0.5 °C) room with the optical settings described above. All image analysis was performed in FIJI[57], and single-molecule localization was performed via ThunderSTORM[58,59].

For the live-cell experiments, *E. coli* MG1655 strain with a rpoC-Dendra2 strain at the endogenous genetic locus (*E. coli* MG1655 rpoC::Dendra2(CamR))[47] was inoculated into fresh Luria-Bertani (LB) medium and incubated overnight at 37 °C while shaking (180 RPM). On the day of the experiment, cells were reinoculated into fresh EZ Rich Defined Media (EZRDM, Teknova) and incubated at 37 °C while shaking (180 RPM) for 1 h. Next, the culture was split into two subcultures, and to one of them, rifampicin was added to a final concentration of 300 µg ml^{-1}. Both cultures were incubated at similar conditions for 1 h and centrifuged for 2 min 3,000*g* afterward. The supernatant was discarded, cell pellets were washed with fresh EZRDM and centrifuged again with similar parameters and the supernatant was discarded. Cell pellets were resuspended in the residual supernatant and 2 µl of cell suspension was placed on 1% EZRDM–agarose pads (see below) for imaging. All image analysis was performed in FIJI[57], and single-molecule localization was performed via ThunderSTORM[58,59].

Low-melting agarose (Merck-Sigma Aldrich) was suspended in fresh EZRDM to a final concentration of 1% and incubated for 12 min at 70 °C until the solution was clear, then the agarose solution was stored at 42 °C for further use. To prepare agarose pads, 100 µl of agarose solution was placed on an indented microscope slide and covered with a coverslip (#1.5, Marienfield), which was prior cleaned overnight with 1 M KOH (Carl Roth) solution, and incubated for 2 h at room temperature. Then, the coverslip was discarded, and the cell suspension was loaded on the solid agarose pad and covered with a new, clean coverslip.

Reporting summary

Further information on research design is available in the Nature Portfolio Reporting Summary linked to this article.

Data availability

All data underlying this study is available at ref. 60. Source data are provided with this paper.

Code availability

The custom TARDIS software used in this manuscript is provided as supplementary data and can be accessed at ref. 39.

References

52. Berglund, A. J. Statistics of camera-based single-particle tracking. *Phys. Rev. E* **82**, 011917 (2010).
53. Philip, J. *The Probability Distribution of the Distance between Two Random Points in a Box. Tech. Rep. Number TRITA MAT 07 MA 10* (TRITA MAT, 1991).
54. Virant, D. et al. A peptide tag-specific nanobody enables high-quality labeling for dSTORM imaging. *Nat. Commun.* **9**, 930 (2018).
55. Edelstein, A. D. et al. Advanced methods of microscope control using µManager software. *J. Biol. Methods* **1**, e10 (2014).
56. Pinkard, H. et al. Pycro-Manager: open-source software for customized and reproducible microscope control. *Nat. Methods* https://doi.org/10.1038/s41592-021-01087-6 (2021).
57. Schindelin, J. et al. Fiji: an open-source platform for biological-image analysis. *Nat. Methods* **9**, 676–682 (2012).
58. Ovesny, M., Křížek, P., Borkovec, J., Švindrych, Z. & Hagen, G. M. ThunderSTORM: a comprehensive ImageJ plug-in for PALM and STORM data analysis and super-resolution imaging. *Bioinformatics* **30**, 2389–2390 (2014).
59. Martens, K. J. A., Bader, A. N., Baas, S., Rieger, B. & Hohlbein, J. Phasor based single-molecule localization microscopy in 3D (pSMLM-3D): an algorithm for MHz localization rates using standard CPUs. *J. Chem. Phys.* **148**, 123311 (2018).
60. Martens, K. J. A. et al. Data underlying the TARDIS manuscript. *Zenodo* https://doi.org/10.5281/zenodo.7900405 (2023).

Acknowledgements

This work was financially supported by funding from a VLAG PhD-fellowship (J.H.), start-up funds at Carnegie Mellon University (B.T., K.J.A.M. and U.E.), the NSF AI Institute: Physics of the Future (NSF PHY- 2020295) (U.E.), start-up funds at Bonn University (B.T., K.J.A.M. and U.E.), an Argelander Starter Kit at the University of Bonn (K.J.A.M.) and the Alexander von Humboldt Foundation (K.J.A.M.). We acknowledge the valuable input from group meetings from all members in the U.E. and J.H. laboratories. We thank M. Deserno (Carnegie Mellon University, Pittsburgh, USA) for helpful discussions on TARDIS' mathematical foundation.

Author contributions

Conceptualization: K.J.A.M. Data curation: K.J.A.M. Formal analysis: K.J.A.M. Funding acquisition: K.J.A.M., J.H. and U.E. Investigation: K.J.A.M. and B.T. Methodology: K.J.A.M., B.T., J.H. and U.E. Project administration: K.J.A.M., J.H. and U.E. Software: K.J.A.M. Supervision: K.J.A.M., J.H. and U.E. Visualization: K.J.A.M. Writing—original draft: K.J.A.M. Writing—review and editing: all authors.

Competing interests

The authors declare no competing financial interests.

Additional information

Extended data is available for this paper at https://doi.org/10.1038/s41592-023-02149-7.

Supplementary information The online version contains supplementary material available at https://doi.org/10.1038/s41592-023-02149-7.

Correspondence and requests for materials should be addressed to Koen J. A. Martens.

Peer review information *Nature Methods* thanks J. Christof Gebhardt and the other, anonymous, reviewer(s) for their contribution to the peer review of this work. Primary Editor: Rita Strack, in collaboration with the *Nature Methods* team. Peer reviewer reports are available.

https://doi.org/10.1038/s41592-023-02149-7

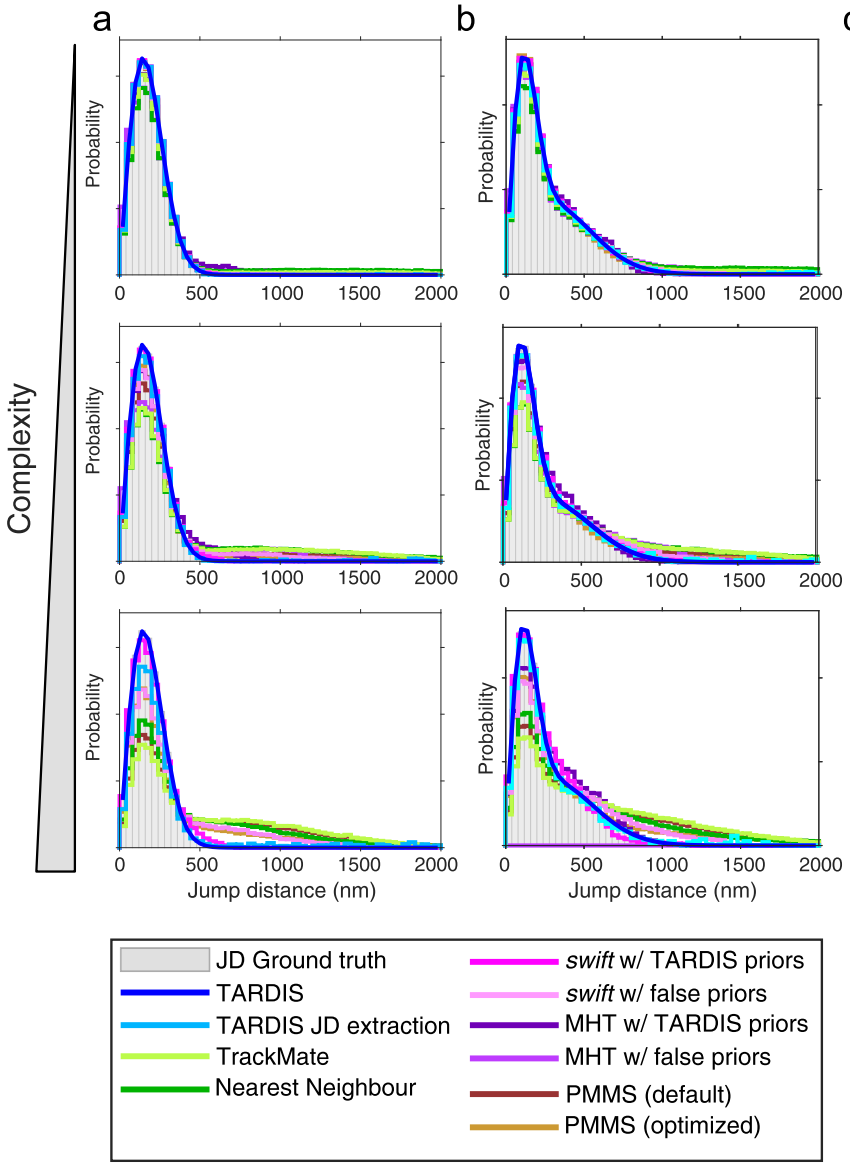

Bhattacharyya distance

One population

Method	Complexity: Low	Medium	High
TARDIS	3.1E-05	4.4E-05	3.5E-05
TARDIS JD extraction	1.7E-03	9.1E-03	3.4E-02
TrackMate	3.1E-02	1.4E-01	2.9E-01
Nearest Neighbour	6.3E-02	1.5E-01	2.0E-01
swift w/ TARDIS priors	1.6E-04	1.6E-03	6.9E-03
swift w/ false priors	2.8E-03	4.3E-02	1.1E-01
MHT w/ TARDIS priors	1.6E-02	2.8E-02	
MHT w/ false priors	3.7E-02	8.6E-02	
PMMS (default)	6.6E-03	8.0E-02	2.5E-01
PMMS (optimized)	8.3E-03	5.3E-02	1.3E-01

Two populations

Method	Complexity: Low	Medium	High
TARDIS	8.5E-05	1.6E-04	1.5E-04
TARDIS JD extraction	4.4E-03	8.0E-03	1.0E-02
TrackMate	1.9E-02	7.4E-02	1.4E-01
Nearest Neighbour	3.9E-02	7.5E-02	8.2E-02
swift w/ TARDIS priors	3.7E-04	2.6E-03	3.1E-03
swift w/ false priors	1.2E-03	9.8E-03	2.6E-02
MHT w/ TARDIS priors	2.4E-03	2.0E-03	5.0E-03
MHT w/ false priors	1.3E-02	2.8E-02	
PMMS (default)	4.8E-03	4.3E-02	1.1E-01
PMMS (optimized)	5.7E-03	2.6E-02	5.5E-02

High similarity to GT — Low similarity to GT

Extended Data Fig. 1 | Performance of TARDIS and spt tracking methods for a single diffusive population and two diffusive populations at increasing complexity, visualised on a linear x-axis. Performance of TARDIS is compared to the blind tracking algorithms uTrack-inspired PMMS (piecewise-stationary motion model and iterative smoothing)[40,42], TrackMate[40,41] and Nearest neighbour analysis, and to the prior-informed methods *swift* (Endesfelder et al., manuscript in prep.), and Multiple-Hypothesis Tracking (MHT)[25] (MHT at the most complex dataset did not run to completion). This data is also presented in Figs. 1c and 2c. (c) Bhattacharyya distance of the distributions in (a) and (b) compared to the ground truth (GT) jump distance distribution, calculated as the negative natural logarithm of the sum of the square root of the product of the distribution value of a method and that of the jump distance ground truth.

https://doi.org/10.1038/s41592-023-02149-7

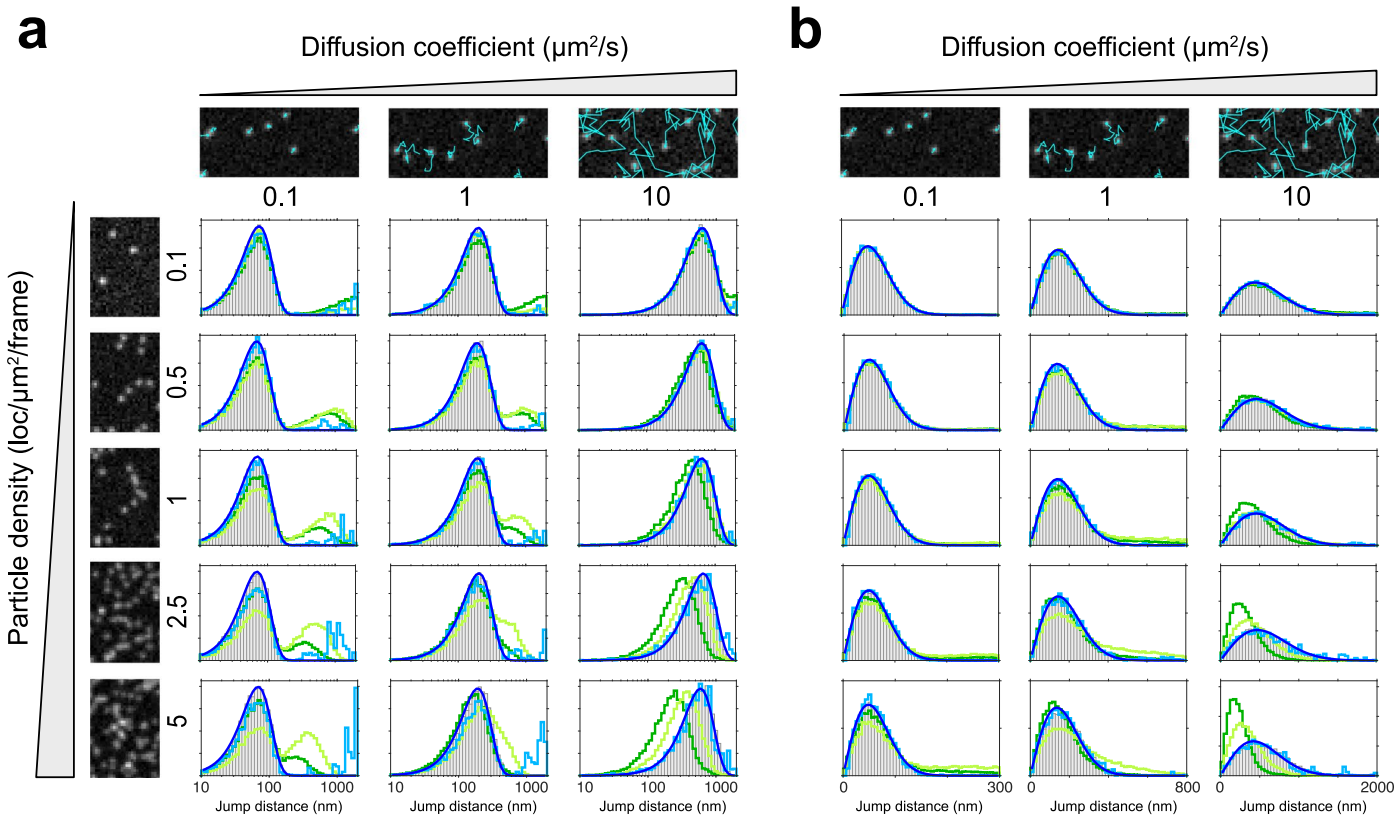

Extended Data Fig. 2 | The full dataset as presented Fig. 2a, analysed via TARDIS (blue), TARDIS-JD-extraction (light-blue), TrackMate-LAP[40,41] (light green) and nearest-neighbour tracking (dark green). (**a**) and (**b**) represent the same datasets, but visualised on a logarithmic (a) or linear (b) x-axis. Note the changing jump distance x-axis scaling in (b). The TARDIS fit data is also presented in Extended Data Fig. 3a.

https://doi.org/10.1038/s41592-023-02149-7

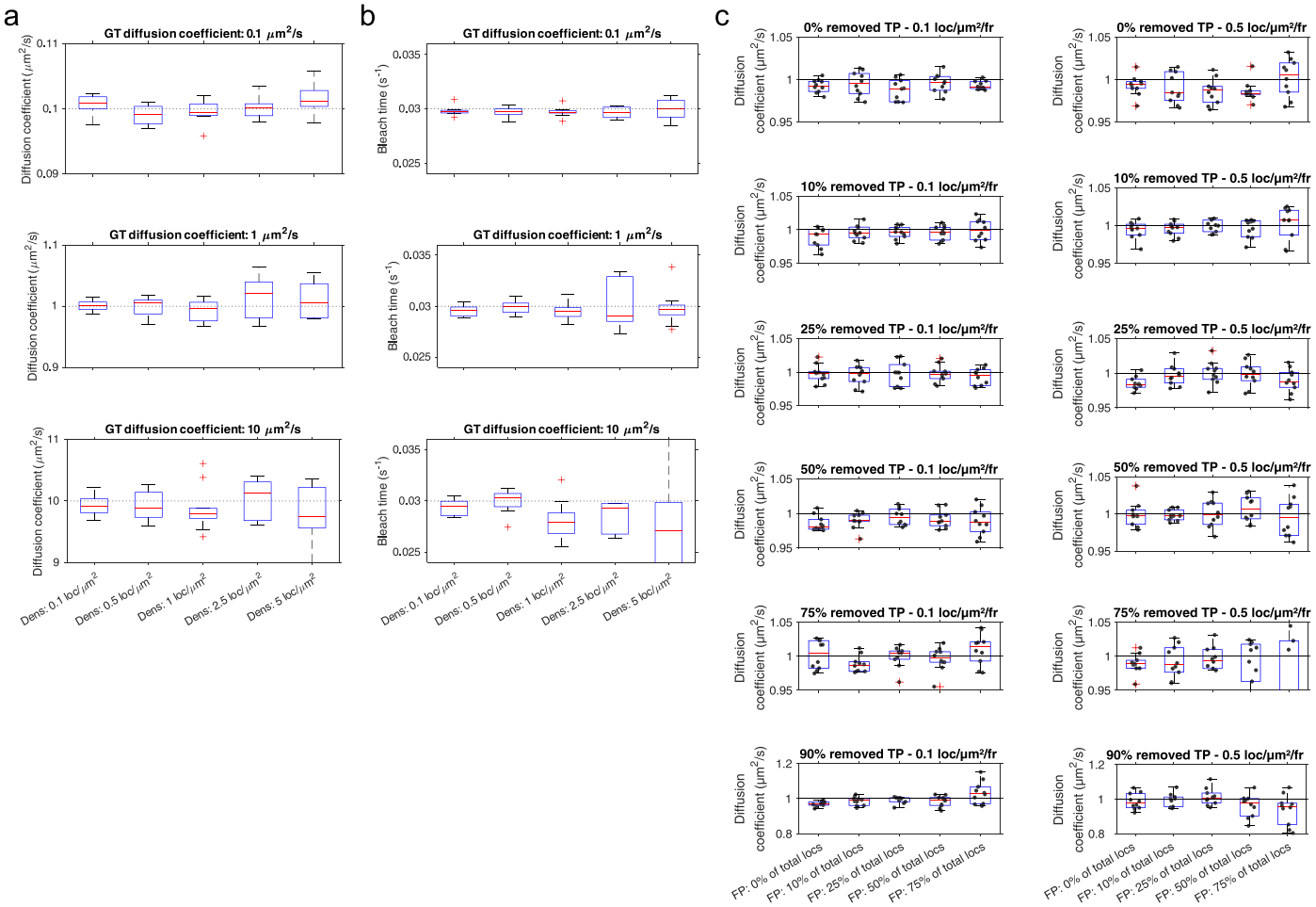

Extended Data Fig. 3 | Detailed information on diffusivity and bleach time obtained from TARDIS fitting. (**a**) Boxplots showing the obtained diffusion coefficients of datasets presented in Fig. 2a, and (**b**) the obtained bleaching times of datasets presented in Fig. 2a, showing no bias in either over the complexity range. TARDIS is repeated 10 times on 20.000 simulated localizations for each condition. (**c**) Individual fit information of data presented in Fig. 2b. For every condition, TARDIS is repeated 10 times on 20.000 simulated localizations with random start positions in TARDIS. The obtained diffusion coefficients are visualised (scatter points represent individual measurements). Note the changing y-axis at 90% removed true positives in (c). Abbreviations used: TP: True Positives, FP: False Positives, fr: frame, locs: localizations. All boxplots show the median as the central mark, with the 25th and 75th percentile as lower and upper edges. Whiskers extend to non-outlier extreme points, and outlier points are plotted as plusses.

https://doi.org/10.1038/s41592-023-02149-7

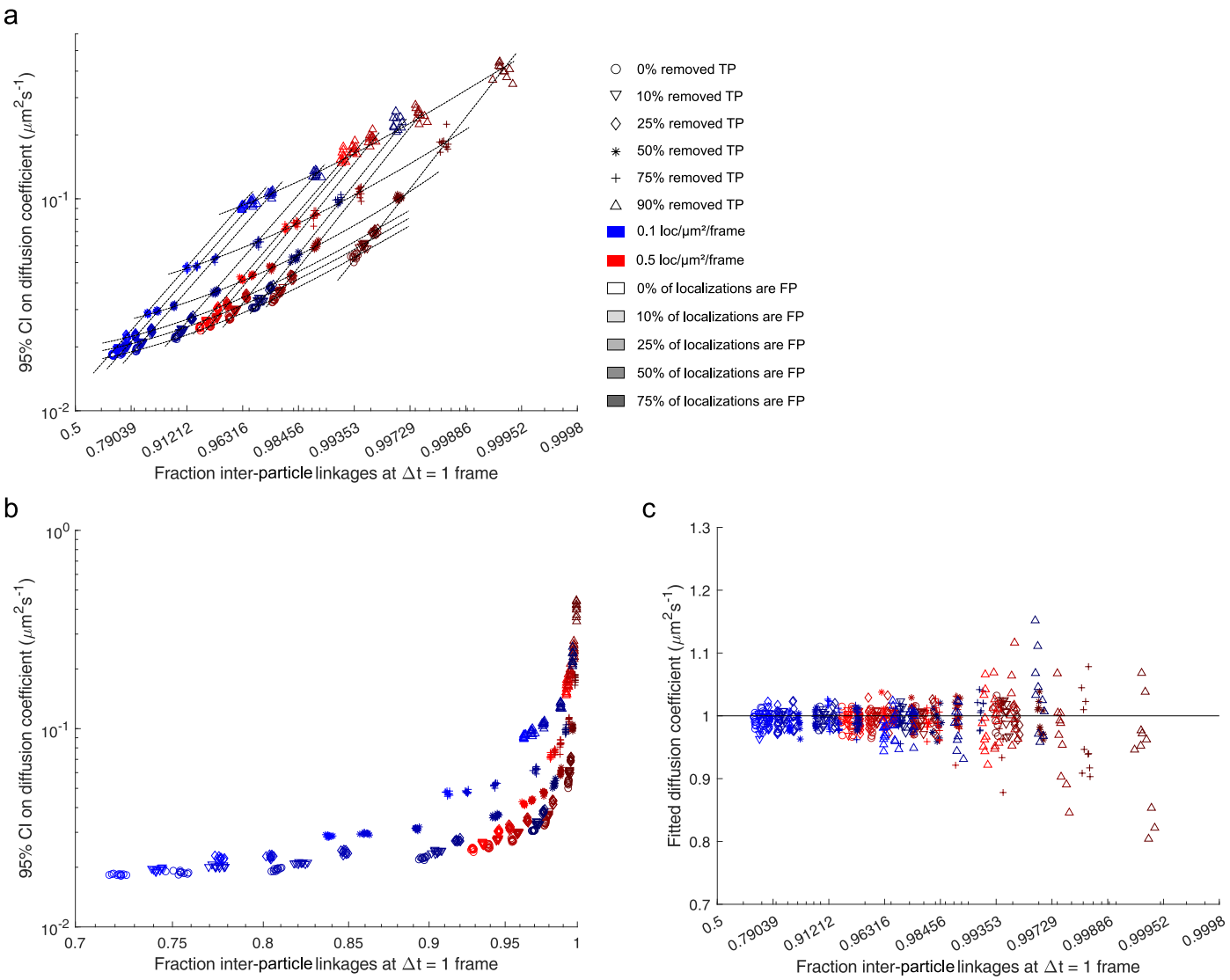

Extended Data Fig. 4 | Detailed information on TARDIS fitting results of bleach time of single diffusive population with added noise and blinking chance. Fit information of bleach characteristics corresponding to the data presented in Fig. 2a,b (main manuscript). For every condition, 10 repetitions were analysed with random start positions in TARDIS. (**a**,**b**) RMSE of the diffusion coefficient (**a**) and bleach half-time (**b**) for all conditions presented in Fig. 2a (**c**) The found diffusion coefficient presented in Fig. 2b is visualised (scatter points represent individual measurements). Note the changing y-axis at 90% removed true positives. TARDIS is repeated 10 times on 20.000 simulated localizations for each condition. All boxplots show the median as the central mark, with the 25th and 75th percentile as lower and upper edges. Whiskers extend to non-outlier extreme points, and outlier points are plotted as plusses. Abbreviations used: TP: True Positives, FP: False Positives, fr: frame, locs: localizations.

https://doi.org/10.1038/s41592-023-02149-7

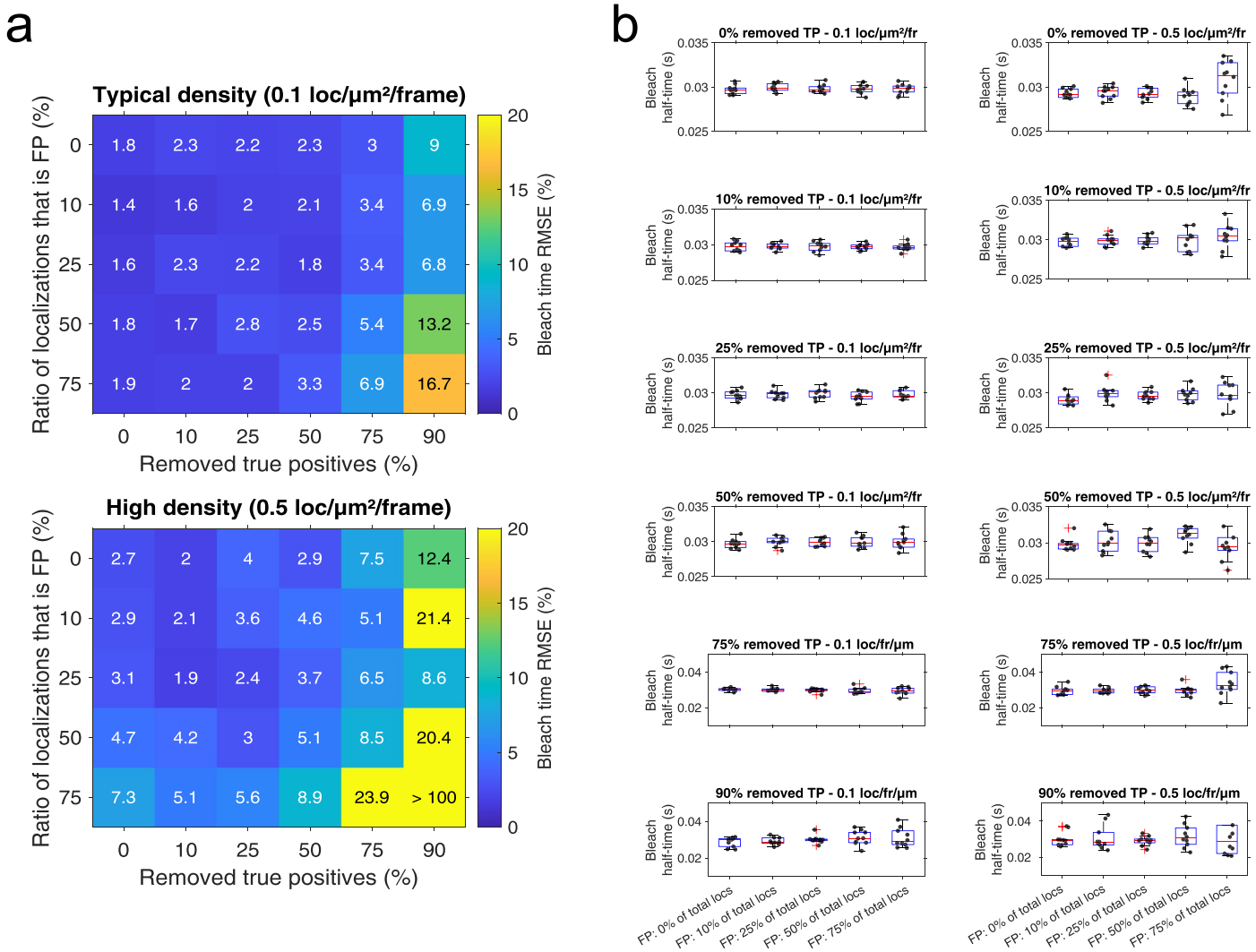

Extended Data Fig. 5 | Effect of the fraction of inter-particle linkages on diffusion coefficient accuracy. Analysis of 95% confidence interval (**a**, **b**), and fitted diffusion coefficient (**c**) as a measure of the inter-particle fraction. Dotted lines in (a) are added for clarity. The underlying analysed data is the same as shown in Fig. 2b. Reasons for increased fraction of inter-particle linkages are clarified via marker type (TP removal), marker colour (TP localization density), and marker darkness (FP introduction). Note that a and c have non-linear x-axis (a and b contain the same information, but with different x-axes).

https://doi.org/10.1038/s41592-023-02149-7

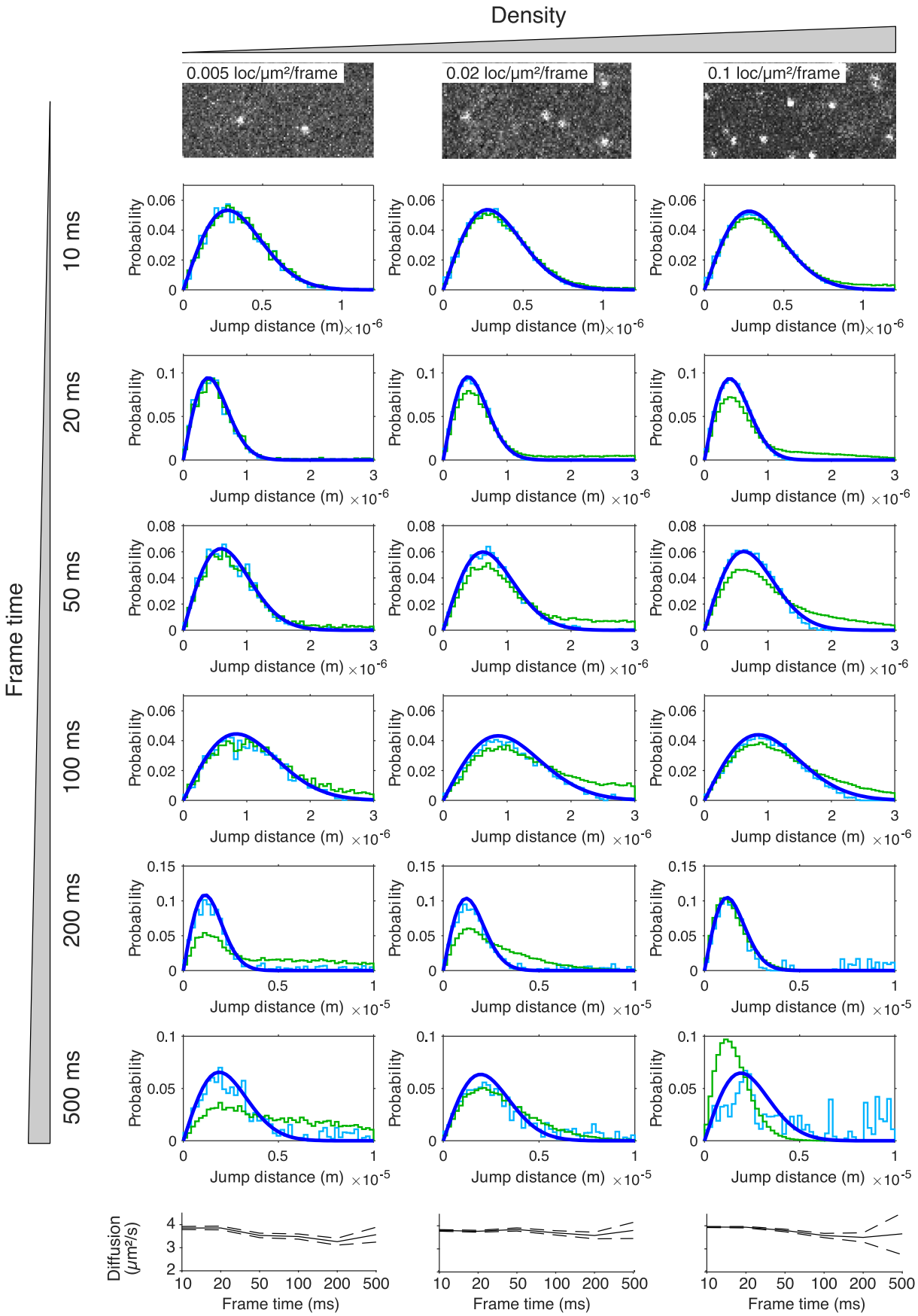

Extended Data Fig. 6 | Diffusion analysis of fluorescent beads at varying frame times. The same information as presented in Fig. 2d, but with additional frame times in between those shown in the main manuscript. The excitation time on every frame is kept constant. The small decrease in obtained diffusion coefficient as a function of frame time is explained by particles having a higher chance to move outside the field-of-view with larger jump distances.

https://doi.org/10.1038/s41592-023-02149-7

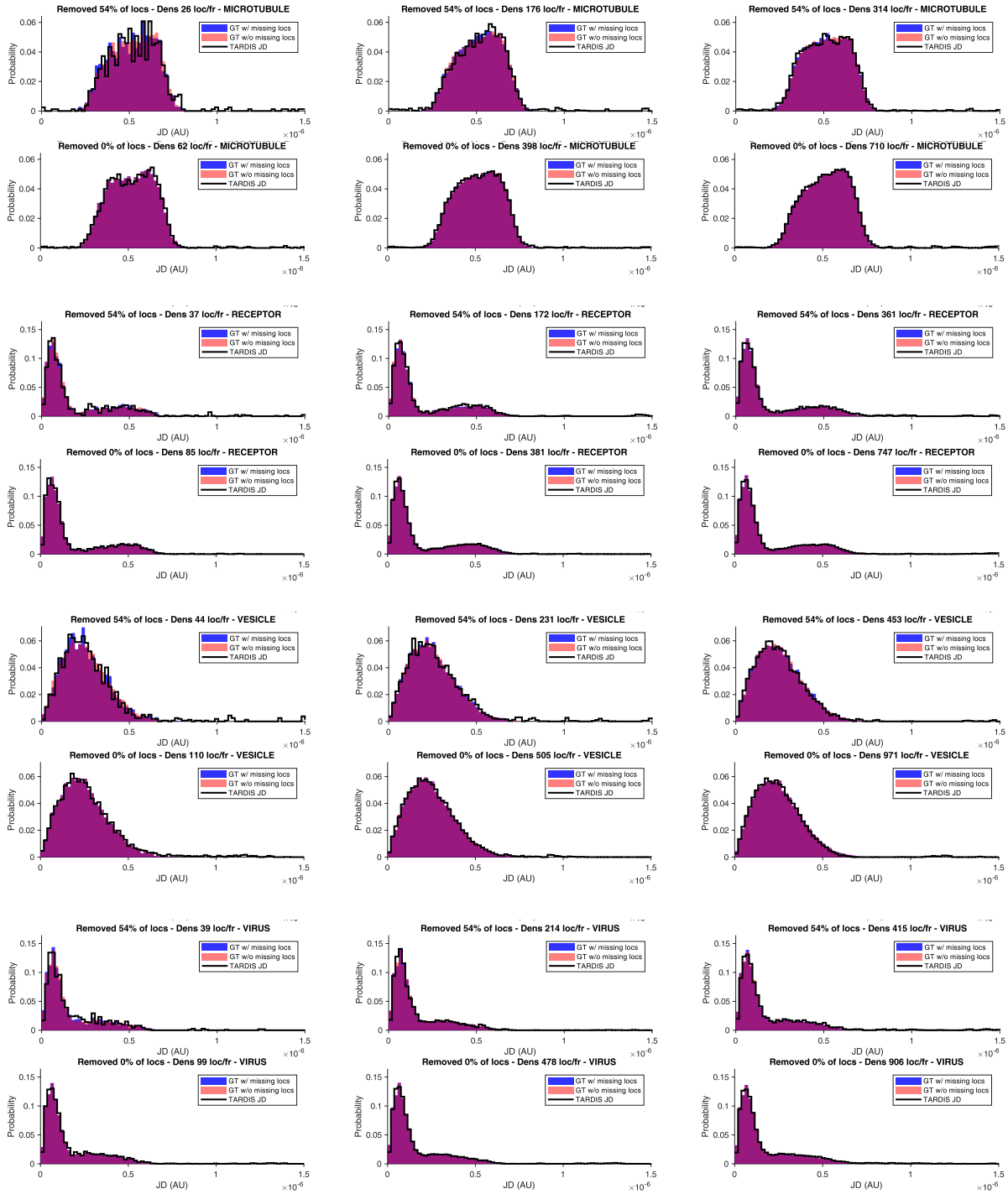

Extended Data Fig. 7 | TARDIS-JD extraction from data of Chenouard et al. Tracking data from Chenouard et al.[23] has been deteriorated (removing 54% of localizations), analysed via the 'extract JD'-function of TARDIS, and compared to the ground-truth (GT) data. Four different conditions are analysed: MICROTUBULE, RECEPTOR, VESICLE, and VIRUS, corresponding to [constant velocity], [tethered motion, switching, any direction], [Brownian motion, any direction], and [same direction dynamics, switching between Brownian and linear] dynamics, respectively. Densities are indicated in subplot titles, while the field-of-view is ~50-by-50 μAU in size. In all scenarios, TARDIS accurately extracts the ground-truth data, and the level of noise is decreasing with decreasing localization removal. The following TARDIS settings were used: Δt bins of 1–3; maximum jump distance of 1e-05 AU; background frames starting at frame-shift of 35, using in total 50 frames; 300 BG bins starting at 3.5e-06 AU.

https://doi.org/10.1038/s41592-023-02149-7

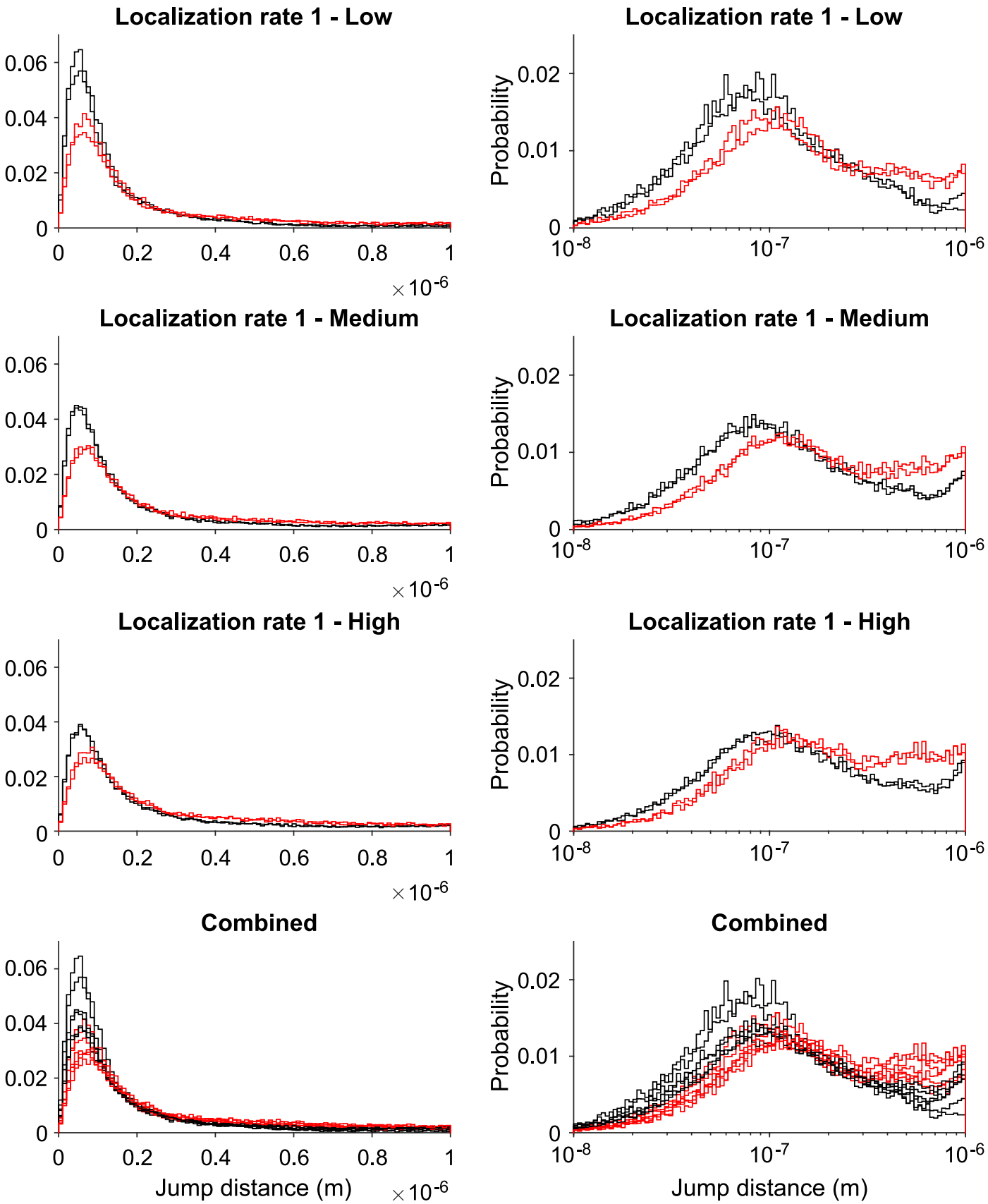

Extended Data Fig. 8 | *E. coli* RNA polymerase jump distance analysis after nearest-neighbour tracking. Jump distance analysis of RNA polymerase in *E. coli* with (red) and without (black) rifampicin, (the same data presented in Fig. 3b), via nearest-neighbour tracking. Notice the changing peak position and abundance as a function of localization density. The data is shown in a linear X-scale (left) and logarithmic X-scale (right).

https://doi.org/10.1038/s41592-023-02149-7

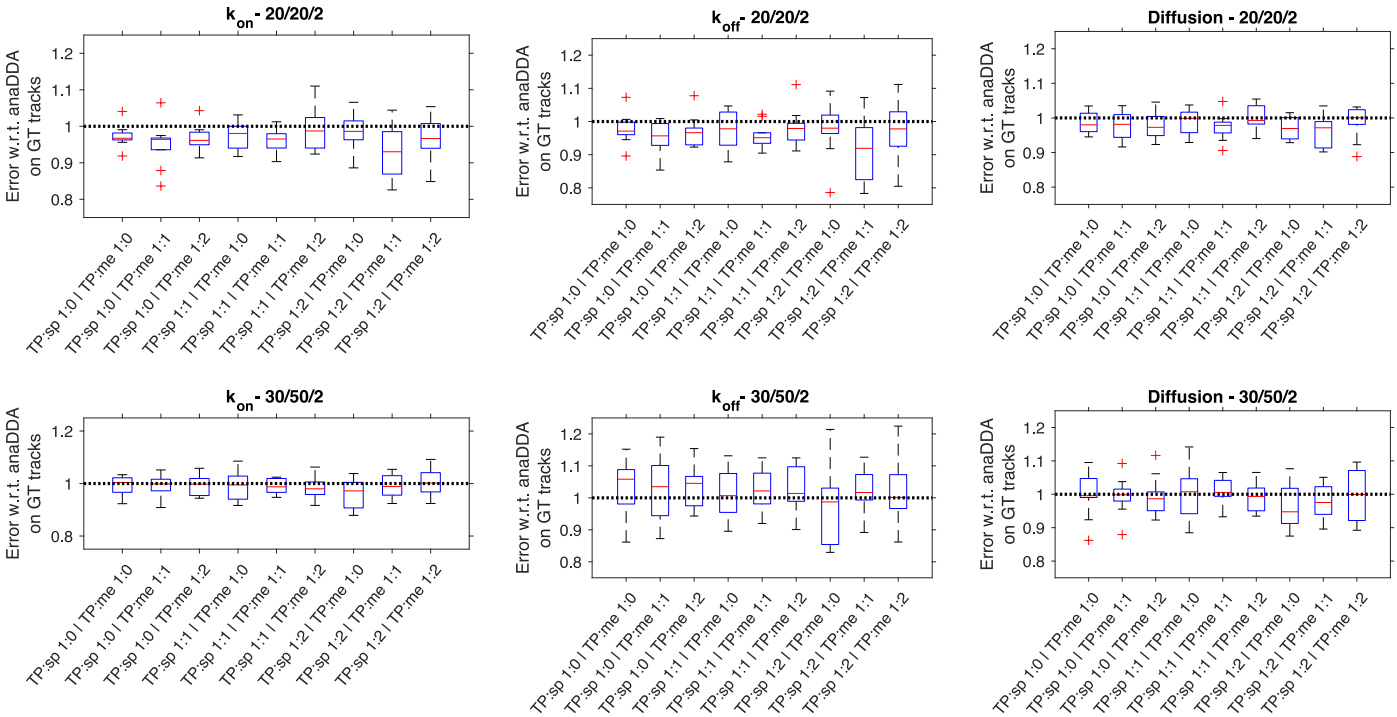

Extended Data Fig. 9 | Detailed information on kinetically state-changing particles. Individual fit information of data presented in Fig. 3c, along with individual fit information for differing binding/unbinding kinetics (titles indicate k_{on} / k_{off} / Diffusion coefficient). For every condition 10.000 'true positive' trajectories were simulated, and 10 repetitions of this were analysed with random start positions in TARDIS, and compared to analysing the same data with anaDDA on the ground-truth trajectory data. TP, *Sp* and *me* indicate true positive, spurious, and membrane localizations, respectively. All boxplots show the median as the central mark, with the 25th and 75th percentile as lower and upper edges. Whiskers extend to non-outlier extreme points, and outlier points are plotted as plusses.

https://doi.org/10.1038/s41592-023-02149-7

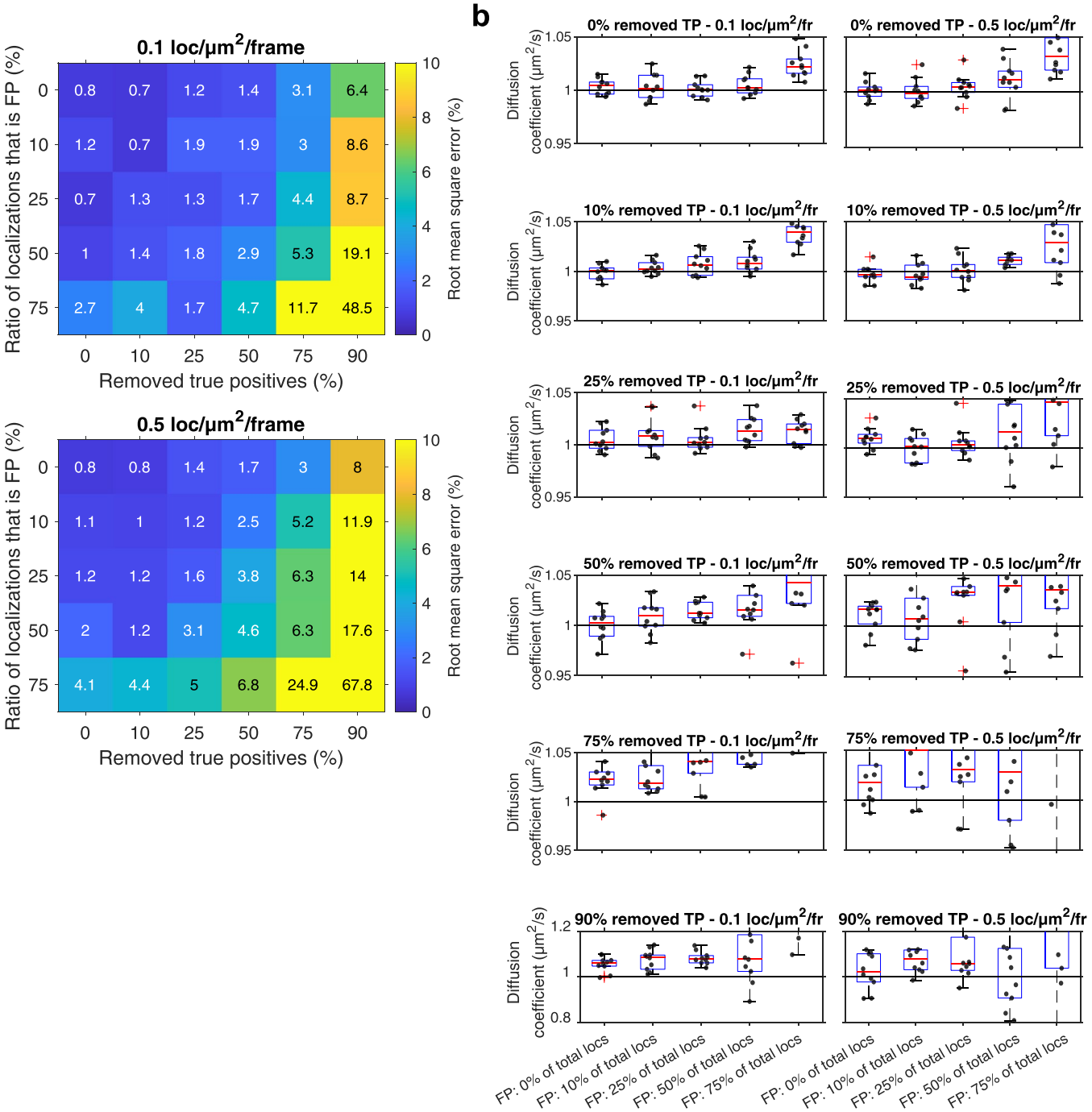

Extended Data Fig. 10 | Accuracy of software by Wolf et al[44]. The same data analysed by TARDIS in Fig. 2b (**a**) and Extended Data Fig. 3b (**b**), analysed via the DANAE software[44], which effectively only performs TARDIS-JD extraction. This is then fitted with a diffusive model afterwards. The accuracy, especially at high complexity scenarios, is worse compared to TARDIS. Additionally, DANAE shows bias towards too high values (right), which is caused by imperfect inter-particle distance distribution subtraction. DANAE is repeated 10 times on 20.000 simulated localizations for each condition. All boxplots show the median as the central mark, with the 25th and 75th percentile as lower and upper edges. Whiskers extend to non-outlier extreme points, and outlier points are plotted as plusses.

nature portfolio

Corresponding author(s): Koen J.A. Martens

Last updated by author(s): Nov 24, 2023

Reporting Summary

Nature Portfolio wishes to improve the reproducibility of the work that we publish. This form provides structure for consistency and transparency in reporting. For further information on Nature Portfolio policies, see our Editorial Policies and the Editorial Policy Checklist.

Statistics

For all statistical analyses, confirm that the following items are present in the figure legend, table legend, main text, or Methods section.

n/a	Confirmed
☐	☒ The exact sample size (*n*) for each experimental group/condition, given as a discrete number and unit of measurement
☐	☒ A statement on whether measurements were taken from distinct samples or whether the same sample was measured repeatedly
☐	☒ The statistical test(s) used AND whether they are one- or two-sided *Only common tests should be described solely by name; describe more complex techniques in the Methods section.*
☐	☒ A description of all covariates tested
☐	☒ A description of any assumptions or corrections, such as tests of normality and adjustment for multiple comparisons
☐	☒ A full description of the statistical parameters including central tendency (e.g. means) or other basic estimates (e.g. regression coefficient) AND variation (e.g. standard deviation) or associated estimates of uncertainty (e.g. confidence intervals)
☐	☒ For null hypothesis testing, the test statistic (e.g. *F*, *t*, *r*) with confidence intervals, effect sizes, degrees of freedom and *P* value noted *Give P values as exact values whenever suitable.*
☒	☐ For Bayesian analysis, information on the choice of priors and Markov chain Monte Carlo settings
☒	☐ For hierarchical and complex designs, identification of the appropriate level for tests and full reporting of outcomes
☒	☐ Estimates of effect sizes (e.g. Cohen's *d*, Pearson's *r*), indicating how they were calculated

Our web collection on statistics for biologists contains articles on many of the points above.

Software and code

Policy information about availability of computer code

Data collection	MicroManager v2.0, PycroManager v0.17.0
Data analysis	TARDISv1.03-1.20 (https://github.com/kjamartens/TARDIS-public), FIJI (ImageJ v 1.53t), ThunderSTORM dev-2018-03-14-pSMLM (Martens et al., 2018), TrackMate v7.10.2. swift v 0.4.3 (availability described in manuscript), ICY v 2.4.3.0, uTrack v 2.3

For manuscripts utilizing custom algorithms or software that are central to the research but not yet described in published literature, software must be made available to editors and reviewers. We strongly encourage code deposition in a community repository (e.g. GitHub). See the Nature Portfolio guidelines for submitting code & software for further information.

Data

Policy information about availability of data

All manuscripts must include a data availability statement. This statement should provide the following information, where applicable:

- Accession codes, unique identifiers, or web links for publicly available datasets
- A description of any restrictions on data availability
- For clinical datasets or third party data, please ensure that the statement adheres to our policy

All data underlying this study is available on doi:10.5281/zenodo.7900405

Human research participants

Policy information about studies involving human research participants and Sex and Gender in Research.

Reporting on sex and gender	N/A
Population characteristics	N/A
Recruitment	N/A
Ethics oversight	N/A

Note that full information on the approval of the study protocol must also be provided in the manuscript.

Field-specific reporting

Please select the one below that is the best fit for your research. If you are not sure, read the appropriate sections before making your selection.

☒ Life sciences ☐ Behavioural & social sciences ☐ Ecological, evolutionary & environmental sciences

For a reference copy of the document with all sections, see nature.com/documents/nr-reporting-summary-flat.pdf

Life sciences study design

All studies must disclose on these points even when the disclosure is negative.

Sample size	Sample size was dictated by microscopy sample (i.e. single fields-of-view were chosen, number of data-points within a field-of-view was dictated). These sample sizes were chosen as they are commonly used in spt(PALM).
Data exclusions	No data was excluded
Replication	RpoC spt was replicated twice per condition
Randomization	Analysis of different datasets was performed identically
Blinding	No blinding was performed, as analysis of different datasets was performed identically

Reporting for specific materials, systems and methods

We require information from authors about some types of materials, experimental systems and methods used in many studies. Here, indicate whether each material, system or method listed is relevant to your study. If you are not sure if a list item applies to your research, read the appropriate section before selecting a response.

Materials & experimental systems

n/a	Involved in the study
☒	☐ Antibodies
☒	☐ Eukaryotic cell lines
☒	☐ Palaeontology and archaeology
☒	☐ Animals and other organisms
☒	☐ Clinical data
☒	☐ Dual use research of concern

Methods

n/a	Involved in the study
☒	☐ ChIP-seq
☒	☐ Flow cytometry
☒	☐ MRI-based neuroimaging